Unraveling Resistance and Thresholds in Phage Therapy Using *Staphylococcus aureus* In Vitro Models

Kévin Royet[1,4], Leslie Blazere[1], Emilie Helluin[1], Ludivine Coignet[1], Lucile Plumet[7], Mélanie Bonhomme[1], Camille Kolenda[1,2], Romain Garreau[4,5,6], Florent Valour[1,3], Mathieu Medina[1], Frédéric Laurent[1,2], Sylvain Goutelle[* 4,5,6]

[1] Equipe Pathogénie des Staphylocoques - Centre International de Recherche en Infectiologie (CIRI), Inserm, U1111, Université Claude Bernard Lyon 1, CNRS, UMR5308, Ecole Normale Supérieure de Lyon, Univ Lyon, F-69007, Lyon, France

[2] Service de Bactériologie, Centre National de Référence des Staphylocoques, Institut des Agents Infectieux, Hospices Civils de Lyon, Lyon, France

[3] Service des maladies infectieuses et tropicales, Hospices Civils de Lyon, Lyon, France

[4] Univ Lyon, Université Claude Bernard Lyon 1, UMR CNRS 5558, Laboratoire de Biométrie et Biologie Évolutive, Villeurbanne, France.

[5] Univ Lyon, Université Claude Bernard Lyon 1, Faculté de Pharmacie de Lyon, Lyon, France

[6] Hospices Civils de Lyon, Groupement Hospitalier Nord, Service de Pharmacie, Lyon, France

[7] Virulence Bactérienne et Infections Chroniques, INSERM U1047, Université de Montpellier, 34095 Montpellier, France

***Corresponding author:** Sylvain Goutelle, Laboratoire de Biométrie et Biologie évolutive, Université Claude Bernard Lyon 1, CNRS, UMR5558, 43 boulevard du 11 Novembre 1918, Lyon, France. E-mail address: sylvain.goutelle@univ-lyon1.fr.

Abstract

Background

Phage therapy is a promising approach against multidrug-resistant *Staphylococcus aureus*, but its clinical development is limited by gaps in pharmacokinetic/pharmacodynamic (PK/PD) understanding, especially concerning phage self-replication and resistance dynamics.

Methods

We combined *in vitro* time-kill assays with PK/PD modeling to study three anti-staphylococcal phages (V1SA019, V1SA020, V1SA022) against two *S. aureus* strains (SH1000 and USA300). A system of differential equations captured the co-dynamics of susceptible, resistant and infected bacteria and free phages. Nonlinear mixed-effect modeling quantified parameter variability. Resistance emergence was monitored through phenotyping and whole-genome sequencing of resistant clones.

Results

Phage–bacteria interactions followed a predator–prey pattern, with early bacterial growth, rapid phage amplification, and subsequent bacterial collapse. However, resistant subpopulations emerged, regrew over time, in a multiplicity of infection (MOI) dependent way. The model accurately described bacterial and phage dynamics and estimated kinetic parameters including adsorption and burst size. Proliferation and inundation thresholds varied by strain and phage. All resistant clones harbored mutations in genes involved in teichoic acid biosynthesis, with associated growth defects. Simulations demonstrated that only phage doses exceeding both susceptible and resistant bacterial inundation thresholds fully suppressed regrowth.

Conclusion

This study provides a quantitative framework for understanding phage–*S. aureus* co-dynamics and resistance emergence. It emphasizes the importance of considering both proliferation and inundation thresholds when designing phage dosing regimens. These findings inform the rational development of phage therapy and support translation toward *in vivo* and clinical applications.

50 **Introduction**

51 The emergence of antibiotic resistance is one of the major public threats requiring the development of
52 new antibiotics or alternative therapeutic strategies. Therapy using bacteriophages (or phages) represents a
53 source of considerable hope [1], [2]. Phage therapy has been developed and used for decades in Eastern
54 countries, while in Western countries it is considered that clinical evidence is currently insufficient to be
55 approved by health authorities. In those countries, phage therapy is only used on a compassionate basis when
56 conventional treatments are ineffective. However, phage therapy is promising and was reported to be life-saving
57 in several cases [3].

58 The limited availability of pharmacokinetic and pharmacodynamic (PK/PD) data, combined with the
59 underdevelopment of mathematical models capable of integrating these parameters, hinders the generation of
60 predictive efficacy data of phage therapy. The PK/PD of phages is very different from that of antibiotics and more
61 complex, since phages can self-replicate in the presence of their target bacteria [4]. The co-dynamics of phage
62 and bacterial populations are characterized by specific thresholds effects. The proliferation threshold refers to
63 the bacterial cells density above which the probability of a progeny phage replicating is greater than the
64 probability of that phage being lost [4]. The inundation threshold corresponds to the phage density above which
65 the probability of a bacterial cell being lysed by a phage is greater than the probability of that same bacterial cell
66 dividing [5]. Quantifying those thresholds is crucial in phage therapy in order to define effective doses: the first
67 ensures immediate action of the phages even without replication, while the second guarantees that local
68 amplification of the phages is possible depending on the bacterial density. This allows the therapeutic strategy
69 to be optimized according to the type and dynamics of the infection.

70 *Staphylococcus aureus* is responsible for various infections, including bacteremia, sepsis, pneumonia,
71 endocarditis and bone and joint infections (BJI). Resistance of *S. aureus* to antibiotics is widespread, with
72 methicillin resistant strains being clinically significant [6]. Because of its ability to form biofilms, this pathogen is
73 also difficult to eradicate in device-associated infections. For those reasons, *S. aureus* is classified as high priority
74 for research and development of new therapeutics by the World Health Organization and is a target of interest
75 for phage therapy [7].

76 The objectives of this study were (i) to describe and quantify the *in vitro* co-dynamics of three candidate anti-
77 staphylococcal phages (V1SA019, V1SA020 and V1SA022) and two reference methicillin susceptible (SH1000) /

78 resistant (USA300) *S. aureus* strains; and (ii) to build a robust mathematical model describing these co-dynamics

79 and that can generate predictive data of phage efficacy.

80

81 **Materials and methods**

82

83 **Experimental method**

84 **Bacterial culture and phage propagation**

85 We used two reference strains of *S. aureus*, SH1000 [8] and USA300 LAC strain [9], as well as three phage
86 candidates, V1SA019, V1SA020 or V1SA022 [10].*S. aureus* strains were grown weekly on Columbia Agar
87 supplemented with 5% Sheep Blood (BioMerieux, Marcy-l'Etoile, France) for 20 h at 37 °C. For culture, one colony
88 was picked with an inoculation loop and suspended in cation adjusted Mueller Hinton (caMH) (Becton Dickinson,
89 Franklin Lakes, NJ, USA), then incubated at 37 °C for 20 h at 180rpm. *S. aureus* bacteriophage V1SA019, V1SA020
90 or V1SA022 were routinely propagated as previously described [10]. Briefly, susceptible bacterial strain in
91 exponential phase and phages were mixed at MOI of 10^{-3} phage per bacteria in 10 mL of Tryptic Soy Broth (TSB,
92 BD, Franklin Lakes, NJ, USA). After 24 h of incubation, the obtained phage lysates were filtered using a 0.22 µm
93 syringe filter and phage titers were measured by spot test assays. For spot test assay, 600uL of overnight culture
94 of a susceptible strain was mixed with 3.5% caMH agar melted and kept at 55°C and then poured in an empty
95 120-mm-diameter petri dish. Finally, phages were serially diluted in PBS, and 5 µL of each dilution were spotted
96 onto plates, which were then incubated for 24 hours at 37 °C prior to plaque-forming unit (PFU) enumeration.

97

98 **Bacteriophage decay**

99 To determine the free phage decay rate in the absence of bacteria, V1SA019, V1SA020 or V1SA022 were added
100 to 25 mL of pre-warmed caMH in 50 mL conical tubes at a final concentration of 10^1 PFU mL^{-1}, 10^3 PFU mL^{-1} or
101 10^5 PFU mL^{-1} and incubated at 37 °C with shaking at 180 rpm. Samples were collected at 3 h, 6 h, 24 h and 48 h
102 and bacteriophages were enumerated using double layer plaque assay [11]. Briefly, 100µL of a phage lysate was
103 mixed with 300µL of bacterial culture in stationary phase and held for 10min at room temperature. Then, 10 ml
104 of 3.5% caMH agar melted and kept at 55°C was added, and, after mixing, the contents of the tube were
105 immediately poured onto a 90-mm-diameter petri dish of caMH agar (BioRad, Hercules, CA, USA). Three
106 independent experiments were performed.

107

108

109 ***In vitro* time-kill experiments**

110 Four series of time-kill experiments were conducted. The effect of the three phages (V1SA019, V1SA020 or
111 V1SA022) was evaluated on the SH1000 strain. In addition, V1SA019 was also tested against the USA300 LAC
112 strain. This allowed to study the variability of the phage-bacteria dynamics between phages and bacterial strains.
113 Optical density at 600nm (OD_{600nm}) of overnight *S. aureus* liquid cultures was measured and an aliquot was added
114 to 25 mL pre-warmed caMH in conical tube (Falcon, Le Pont de Claix, France, 50 mL) to a final concentration of
115 10^3 colony-forming units (CFU) mL^{-1} and incubated at 37 °C under microaerobic condition with shaking at 180
116 rpm. After 1 h of lag phase, bacteriophages V1SA019, V1SA020 or V1SA022 were added to a final concentration
117 of 10^1 plaque-forming units (PFU) mL^{-1}, 10^3 PFU mL^{-1} or 10^5 PFU mL^{-1} to give an approximate multiplicity of
118 infection (MOI) of 0.01, 1 or 100. Samples were taken every 2 h for 24 h, serially diluted and plated on caMH agar
119 plates for bacterial enumeration. Undiluted samples were also spread on caMH agar to lower down the detection
120 limit to 4 CFU mL^{-1}. Each aliquot was then centrifuged for 30s at 20,000g to remove *S. aureus* cells and
121 supernatant was diluted for bacteriophages enumeration by spot test or double layer plaque assays when
122 applicable (i.e., when estimated PFU $mL^{-1} < 2.2 \times 10^2$). At the end of the experiment, 1mL of culture was stored
123 at -80°C in culture medium with 20 % glycerol to allow subsequent isolation of bacteria. Experiments were
124 performed using three different phage production batches infecting tree independent bacterial cultures for each
125 MOI. All experiments were conducted in triplicates on different weeks.
126
127 **PK/PD modeling**
128 We used a population approach and nonlinear mixed effect modeling to describe the time course of bacteria and
129 phage counts in all four sets of experiments. Time-kill, bacterial growth and phage decay data were analyzed.
130 However, adsorption and burst-size data could not be included in the final model, as preliminary runs showed
131 model instability and unrealistic estimates. Nevertheless, adsorption and burst size assays are described in
132 supplementary methods and results are shown in Table S1, S2 and Figure S1, S2.
133 A model written in ordinary differential equations (ODE) was implemented in the Monolix software (version
134 2024, Lixoft, Antony, France) to describe the interactions between four populations: susceptible bacteria (S),
135 resistant bacteria (R), bacteria infected by phages (I) and free phage viruses (V). The ordinary differential
136 equations corresponding to this model were as follows (Equation 1):
137

$$\begin{cases} \frac{dS}{dt} = \alpha \times \left(1 - \frac{S}{B_{max}}\right) \times S - mut \times S - bind_S \times S \times V \\ \frac{dR}{dt} = \alpha \times \left(1 - \frac{R}{B_{max}}\right) \times R + mut \times S - bind_R \times R \times V \\ \frac{dI}{dt} = bind_S \times S \times V + bind_R \times R \times V - Lysis \times I \\ \frac{dV}{dt} = burst \times Lysis \times I - bind_S \times S \times V - bind_R \times R \times V - decay \times V \end{cases} \qquad (Eq. 1)$$

The eight parameters were:

α: bacterial growth constant; Bmax: maximal concentration of bacteria; mut: mutation rate of S to R bacteria; $bind_S$ and $bind_R$: binding rate constant of phages to S and R bacteria respectively; lysis: lysis rate constant of I bacteria; burst: number of free phages released upon I bacteria burst; decay: elimination rate constant of free phages

This model was inspired by previously published *in vitro* PK/PD studies [5], [12] and is schematically described in Figure 1. Inclusion of resistant bacteria was necessary to describe bacterial regrowth observed *in vitro*. For each parameter, both fixed (median, typical value) and random (inter-experiment variability) effect parameters were estimated, within a general framework as follows:

$$\vartheta_i = TV(\vartheta) * exp(\eta_i) \qquad (Eq. 2)$$

With

$$\eta_i \sim (0, \omega^2) \qquad (Eq. 3)$$

Where θi is the parameter value (e.g., bacteria growth rate, phage decay…) for an individual experiment, TV(θ) is the typical parameter value in the whole set of experiments, i.e. the median for a lognormal distribution (considered as a fixed effect in the nonlinear mixed effects model), and η_i is a random effect variable quantifying the variability around the typical value. Random effects were assumed to follow a normal distribution with mean of zero and variance ω^2. As a result of Equation 2, parameters (θ_i) are assumed to follow a log-normal distribution.

Model outputs were coded as $\log_{10}(S + R + I)$ and $\log_{10}(V)$ for bacteria and virus, respectively, to facilitate comparison with observations. Several residual error models were evaluated, including additive, proportional and combined error models. The production batch was evaluated as a potential descriptor of inter-experiment variability.

Model evaluation was based on goodness-of-fit criteria including objective function (-2 x log-likelihood) and Akaike Information Criterion (AIC). Plots of observed versus model individual estimates were examined, as well as distributions of individual weighted residuals. Visual predictive checks based on 1000 simulations were performed as internal validation. Because proliferation and inundation thresholds are not primary parameters but combination of ODE parameters [5], they were not estimated at the population level but computed for each experiment after Bayesian estimation of individual parameters and summarized with descriptive statistics.

The proliferation thresholds of phages for susceptible and resistant bacteria ($Prolif_S$ and $Prolif_R$) were calculated as follows [5] :

$$Prolif_S = \frac{dec}{bind_S \times (burst - 1)} \qquad (Eq.\ 4)$$

$$Prolif_R = \frac{dec}{bind_R \times (burst - 1)} \qquad (Eq.\ 5)$$

The inundations thresholds for susceptible and resistant bacteria ($Inund_S$ and $Inund_R$) were calculated as follows [5]:

$$Inund_S = \frac{alpha - mut}{bind_S} \qquad (Eq.\ 6)$$

$$Inund_R = \frac{alpha}{bind_R} \qquad (Eq.\ 7)$$

Finally, simulations were performed based on the final model for V1SA019 / SH1000 to study the influence of phage MOI on antibacterial effect.

190 **Liquid phage susceptibility test**

191 From *S. aureus* clones isolated and grown on COS agar plates, a colony was resuspended in a 96-well plate
192 containing 200 µL of caMH alone or with 10^6 PFU mL^{-1} of phage. Plates were incubated at 37 °C using LogPhase
193 600 under agitation (Agilent BioTek, Santa Clara, USA), and OD_{600} measurements were taken every hour for 24 h.
194 A clone was defined as resistant when its optical density at 600 nm after 24 hours of incubation exceeded 0.1, in
195 contrast to the negative control (wild-type SH1000 inoculated in the presence of the phage), which showed no
196 detectable growth under the same conditions.

197

198 **DNA extraction and sequencing**

199 Bacterial DNA was extracted using the Maxwell® RSC Blood DNA kit (Promega, Madison, WI, USA), after an initial
200 incubation with 40 µg lysostaphin (Sigma-Aldrich, Saint Louis, MO, USA Aldrich), 200 µg lysozyme (Sigma-Aldrich)
201 and 200 µg RNaseA (Qiagen, Hilden, Germany) for 1 h at 37 °C, followed by incubation with 12 mAU (AU= Anson
202 unit) of proteinase K (Promega) for 20 min at 60 °C. Whole genome sequencing was performed with NextSeq
203 instrument (Illumina, San Diego, CA, USA) using a 150 bp paired-end protocol. Reference genome assembly was
204 performed using SPAdes v3.15.5 [13] and Bakta v1.7.0 [14] was used for genome annotation. SNPs analysis was
205 conducted with snippy v4.6.0 (https://github.com/tseemann/snippy). Indels were found with mummer4 v4.0.0
206 [15].

207

208 **Assessment of the fitness of phage-resistant clones**

209 The relative fitness of phage-resistant clones was assessed by comparing their growth dynamics to that of the
210 wild-type strain. Strains were pre-cultured overnight in caMH medium at 37°C, then diluted to an initial OD_{600} of
211 0.01 in fresh caMH medium. Cultures were transferred to 96-well microplates and incubated at 37°C with
212 continuous orbital shaking. OD_{600} measurements were recorded hourly using a Tecan Infinite M200 Pro plate
213 reader. Each condition was tested in four independent biological replicates, each comprising three technical
214 replicates.

215

216 **Statistical analysis of experimental data**

Statistical analyses and plotting were performed using GraphPad Prism, version 8.0.0 (GraphPad Software, San Diego, CA, USA). Variables were compared using the nonparametric Mann-Whitney U test. A p-value < 0.05 was considered significant.

222 **Results**

223

224 **Phage decay**

225 Without bacteria, phages declined linearly on the log-scale (Figure 2). The loss of phage viability over 24 h was
226 low (mean ratio < 10 PFU.mL^{-1} between 0 - 24 h) for all the concentrations tested, although significant for
227 inoculum values of 10^1 PFU mL^{-1} and 10^5 PFU mL^{-1} of V1SA019, V1SA020 and V1SA022. Over 48 h, phage decay
228 was larger, with mean ratios of phage decay between 0 h and 48 h of 5.4, 3.6, 3.2 for V1SA019; 7, 27, 39 for
229 V1SA020; 9, 34, 43 for V1SA022 for inoculum of 10^1 PFU.mL^{-1}, 10^3 PFU.mL^{-1} and 10^5 PFU.mL^{-1}, respectively.

230

231 ***In vitro* time-kill studies**

232 Phage-bacteria kinetic experiments were conducted at MOIs of 0.01, 1 and 100. We observed a consistent
233 pattern of evolution of bacteria and phage counts (Figure 3). The exponential growth of bacteria was followed
234 by a rapid proliferation of phages. Then, the bacterial population collapsed between 6 and 10 h, while the phage
235 population reached a plateau. An exception to this regular pattern was observed for experiments conducted with
236 V1SA019 on USA300 at MOI of 0.01 where bacterial collapse was observed later, after about 18-20 h and slight
237 decline of phage population was visible at 10-12 h. In several experiments, a regrowth of bacteria was observed,
238 suggesting emergence of bacterial resistance. Regrowth rate appeared to increase with increasing MOI, which
239 was confirmed by the modeling (see below). The final phage concentration was about 10^9 - 10^{11} PFU.mL^{-1}
240 depending on the phage/bacteria couple considered, irrespective of MOI. A slight decline of phage plateau was
241 visible for V1SA019 on SH1000, especially for MOI of 100.

242

243 **Population PK/PD modeling**

244 The *S. aureus* SH1000 / phage V1SA019 pair was used as an illustration for the PK/PD modeling in the manuscript,
245 while results for the other bacteria/phage pairs are provided as supplementary material.

246 The four-equation, eight-parameter model fitted individual bacteria and phages data very well, as shown in
247 Figure 4 for the V1SA019 / SH1000 pair, and supplementary Figure S3 and S4 for the other pairs. Model
248 parameters are shown in

249 for the SH1000 / V1SA019 pair and summarized in supplementary Table S3 for all experiments. The phage
250 production batch showed no influence on PK/PD parameters in all four models. There were minor differences in
251 the final model between the four experiments, regarding Bmax parameter (fixed for V1SA019 / SH1000 Table 1
252 Line 2, random for the other pairs; Table S3 Line 2) and the error model (Table 1 Line 16, 17, 18; Table S3, Line
253 17, 18, 19). Overall, most parameters were estimated with acceptable precision (relative standard error < 50 %,
254 Table 1), including inter-experiment variability. Large imprecision was observed for the median mutation rate
255 (except for V1SA019 / SH1000 pairs, Table 1 Line 3; Table S3 Line 3). This was likely due to the high
256 interexperiment variability of this parameter (high omega values, Table S3 Line 11). A common feature between
257 the four models was a phage binding rate of resistant bacteria ($bind_R$) lower than that for susceptible bacteria
258 ($bind_S$) (Table 1 and S3, Line 4 and 5), resulting in higher proliferation and inundation thresholds for resistant
259 compared to susceptible bacteria (Table 1 Line 19 to 23; Table S3, Line 20 to 24). Also, the estimated typical burst
260 size was larger than the values directly obtained from experimental data (Figure S2, Table S2,Table 1 and Table
261 S3 Line 7). By comparing the results obtained for the SH1000 strain with the three phage candidates (V1SA019,
262 V1SA020, V1SA022), differences between phages can be observed in terms of mutation rate, burst size and decay
263 (Table S3 Line 3, 7, 8). The comparison of the V1SA019 / SH1000 and V1SA019 / USA300 model parameters also
264 revealed differences associated with the bacterial strains. Compared to the SH1000 strain, the USA300 strain
265 displayed a 10-fold lower estimated median burst size and much lower median mutation rate (Table S3, Line 7
266 and 3). However, considerable variability was observed for the mutation rate for the V1SA019 / USA300
267 experiments, with values ranging from 0 to 5.25×10^{-8} between experiments (median = 1.26×10^{-13}) (Table S3,
268 Line 3).

269 Visual predictive checks shown in

270 Figure **5** for V1SA019 / SH1000 supported internal validation of the model. Those plots also exhibited different
271 patterns of bacterial dynamics, including a sharp decline followed by regrowth of total bacteria count after 10-
272 12 h, with variable slopes. Another pattern of constant growth up to a maximum value corresponded to control
273 experiments conducted with bacteria only (no phage).

274 The model also well described the time-course of the bacteria and phage counts of individual experiments. A
275 selection of individual fits for various initial MOIs is shown in Figure S5 for our reference pair V1SA019 / SH1000.
276 Those plots illustrate the bacterial regrowth that appeared to increase with increasing phage dose. This was

277 confirmed by simulations performed with the final model parameters for various phage doses, shown in Figure
278 6. While regrowth was generally limited for an initial MOI of 0.01, it was dramatic for initial MOIs of 1 and 100.
279 Bacterial regrowth rate appeared to be dependent on the initial phage concentration. Such regrowth was driven
280 by the emergence of the resistant bacterial population to phages. However, a phage dose above the inundation
281 threshold (10^{10} PFU mL^{-1}) resulted in very fast killing of all bacteria and no regrowth according to simulations.

282

283 **Emergence of a resistant bacterial subpopulations**

284 At the end of the experiments between V1SA019 and SH1000, one clone from each of the replicates of the three
285 initial MOIs (i.e. three clones per MOI) were randomly selected, isolated, purified and sequenced. Resistance to
286 V1SA019 was confirmed using the spot test assay with no lysis observed. Fitness of phage-resistant clones was
287 assessed in comparison with the wild-type strain after overnight growth in caMH medium. Phage-resistant clones
288 exhibited a delayed onset of exponential growth and reached a lower final OD_{600} compared to the wild-type
289 (Figure S6). Each clone carried at least one mutation (non-synonymous or deletion) in one of the genes involved
290 in the teichoic acid biosynthesis pathway, namely *tarA, tarK* or *tagO*, according to the KEGG pathway (KEGG
291 pathway database) (Table S4).

292 The model predicted the appearance of resistant bacteria as early as 8 h after infection, irrespective of the initial
293 MOI. After 8, 10, 12, 14 and 24 h of infection, up to 60 clones per time were isolated and tested for susceptibility
294 to phage V1SA019 via the liquid phage susceptibility test. At 8 h, 0 %, 7 % and 7 % (60, 27 and 30 clones tested)
295 resistant clones were identified for MOI of 0.01, 1 and 100 respectively. At 10 h, 0 %, 0 % and 19 % (60, 15 and
296 27 clones tested) resistant clones were identified for MOI of 0.01, 1 and 100 respectively. At 12h, 0 % resistant
297 clones were identified for MOI of 0.01 and 1 (30 and 22 clones tested) but this percentage increased to 33 % and
298 100 % (3 and 10 clones tested) at 14 h for MOI 0.01 and 1 respectively. At 24 h, 96 % of resistant clones were
299 identified for MOI of 0.01 and 100 % for MOI of 1 and 100 (24, 30 and 30 clones tested respectively) (Table S5).

300

Discussion

Co-dynamics of bacteria and phage

We combined *in vitro* experiments and mathematical modeling to investigate the co-dynamics between two *Staphylococcus aureus* strains and three candidate phages [10] across three MOIs. *In vitro* experiments revealed the emergence of a phage-resistant subpopulation across all phage–bacteria pairs tested. According to the mathematical model, this resistant subpopulation exhibited a reduced phage adsorption rate compared to susceptible bacteria, as well as distinct values for proliferation and inundation thresholds.

Our analysis confirmed that the co-dynamics between phages and bacteria can be effectively described using ODE, capturing predator–prey-like interactions. The model was inspired by the framework developed by Cairns and colleagues [5], and builds upon previous mathematical approaches established through *in silico* and *in vitro* studies of pathogens such as *Salmonella typhimurium* and *Campylobacter jejuni* [5], [12], [16], [17], [18], [19]. While probabilistic models—such as logistic regression approaches—have been applied to predict *S. aureus* inactivation by phages in matrices like pasteurized milk [20], to our knowledge, no ODE-based model has yet been developed to characterize the dynamic interactions between *S. aureus* and lytic phages under laboratory conditions. In addition, we employed a non-linear mixed-effects modeling approach to quantify experimental variability in pharmacokinetic/pharmacodynamic (PK/PD) parameters. This allowed us to capture substantial inter-experimental variability, particularly in mutation rate and phage burst size. It is worth noting that the estimated median mutation rate (2.64×10^{-9} / h) is consistent with previously reported *in vitro* mutation rates for *S. aureus* populations, which range from 1×10^{-8}/h to 5×10^{-9} / h.

A key strength of our study lies in the simultaneous investigation of three distinct phage candidates and two *Staphylococcus aureus* strains. Our findings highlight notable differences in key dynamic parameters, particularly between the SH1000 and USA300 strains. These results suggest that phage–bacteria interaction dynamics are highly pair-specific and cannot be reliably generalized or extrapolated from a single strain–phage combination.

325 **Proliferation and inundation thresholds**

326 The model enabled estimation of the inundation and proliferation thresholds that define two distinct modes of
327 phage therapy—passive and active, respectively [4], [21]. In passive therapy, a sufficiently high initial phage dose
328 ensures immediate bacterial clearance, while in active therapy, therapeutic success relies on *in situ* phage
329 amplification following bacterial infection. *In vitro* time-kill assays showed that bacterial growth persisted in the
330 presence of lytic phages until the inundation threshold was reached, at which point rapid bacterial killing
331 occurred. Previous models estimated the minimum phage concentration required to inactivate *S. aureus* in milk
332 at approximately 8 $\log_{10}$ PFU mL^{-1} [20], a value closely matching the inundation thresholds calculated in the
333 present study (8.0 to 8.7 $\log_{10}$ PFU mL^{-1}), despite differing experimental conditions. In contrast, the proliferation
334 threshold was more difficult to discern from time-course data, as previously noted by Cairns *et al*. [5], particularly
335 since only free phages were quantified. Despite this limitation, our study relied on free phage measurements to
336 estimate the proliferation threshold, which for susceptible bacteria ranged from 4.5 to 5.2 $\log_{10}$ CFU mL^{-1} and
337 appeared independent of the phage, the initial phage dose, or the bacterial strain.

338

339 Although these thresholds may vary under different *in vitro* and *in vivo* conditions, this study demonstrates that
340 in the context of active phage therapy, a minimal bacterial population is necessary to enable phage amplification,
341 reach the inundation threshold, and ultimately reduce bacterial load [22]. This might suggest that different phage
342 doses below the inundation threshold would produce similar bacterial load dynamics; however, this assumption
343 is incorrect. Our results show a clear effect of the initial phage dose—still below the inundation threshold—on
344 both the average final abundance of resistant bacteria and their growth rate. This phenomenon was observed
345 consistently across all phage–bacteria pairs studied. Under certain conditions (e.g., phage V1SA019 infecting
346 SH1000 at a MOI of 0.01), complete absence of resistant bacteria could be observed at the end of the experiment.
347 This effect may result from the use of a closed culture system. Delayed control of the susceptible bacterial
348 population at lower MOI leads to greater depletion of the culture medium, which was not replenished during
349 our experiments, due to extensive and prolonged bacterial replication. Consequently, resistant bacteria
350 emerging at low MOI encounter a less favorable environment for growth.

351

352 The correlation between bacteria regrowth and initial MOI is intriguing. Our simulations performed with various
353 MOIs provided interesting insights (Figure 6) and suggested the importance of achieving the inundation threshold
354 of the resistant subpopulation for controlling the regrowth with active phage therapy. For the lowest MOI (0.01),
355 it took longer for the phage population to achieve the inundation threshold of susceptible bacteria. This leaves
356 more time for susceptible bacteria to grow, and the susceptible bacteria peak is the highest, compared with
357 higher MOI. The phage population plateau is also higher, close to the inundation threshold of resistant bacteria
358 estimated at 4 x 10^{10} PFU ml^{-1} (median). By contrast, higher MOI result in lower susceptible bacteria peak and
359 lower phage plateau, below the inundation threshold of resistant bacteria. Based on those observations, we
360 assume that two ways exist to prevent the emergence of resistant bacteria and prevent bacteria regrowth in
361 such *in vitro* conditions. The first one is to use a very high dose of phage, greater that the inundation threshold
362 of susceptible bacteria that totally suppress the mutation process (passive therapy). The other option is to use
363 active therapy with a phage dose that permits phage amplification up to the inundation threshold of resistant
364 bacteria.

365 For phage doses exceeding the inundation threshold (passive therapy), bacterial concentrations are rapidly
366 reduced due to lysis of the majority of susceptible cells. Although our simulation results indicate that
367 administration of a phage dose above this threshold is necessary for rapid bacterial clearance without the
368 emergence of resistance, reaching such high phage concentrations may be challenging due to formulation
369 constraints and accessibility at the infection site. Furthermore, passive therapy may not achieve complete
370 eradication, leaving a residual susceptible bacterial population with a reduced probability of encountering
371 phages [23], [24]. Consequently, phage concentrations at the infection site may decline, allowing bacterial
372 regrowth until the proliferation threshold is reached, thus enabling active therapy if viable phages remain. Obeso
373 *et al*. reported that the efficacy of phage-mediated *S. aureus* inactivation in milk is influenced by the initial
374 bacterial load, likely related to the bacterial proliferation threshold [20]. In contrast, Bigwood *et al.* demonstrated
375 that biocontrol of low levels of *S. typhimurium* in liquid foods is achievable by applying sufficiently high phage
376 concentrations, independent of initial pathogen counts [19]. Therefore, optimal phage dosing must balance
377 immediate bactericidal efficacy with long-term control outcomes.

378

379

380 **Emergence of a resistant bacterial subpopulation**

381 All nine clones isolated 24 h post-infection harbored mutations in genes involved in the teichoic acid biosynthesis
382 pathway, which encodes the primary receptor for phages in *S. aureus* and, more generally, in Gram-positive
383 bacteria [25], [26]. This finding indicates that, despite variations in bacterial population control across MOI
384 conditions, phage-induced selective pressure consistently drives a similar adaptive response. Nonetheless, all
385 resistant clones exhibited a growth defect when tested individually in caMH medium, suggesting a fitness cost
386 that may facilitate their elimination by the host immune system, as previously observed in *in vivo* models of *S.*
387 *aureus* under phage predation [27], [28]. Clones isolated at intermediate time points during the kinetics were
388 not sequenced, and the presence of mixed subpopulations during these phases cannot be ruled out. Liquid
389 susceptibility tests using V1SA019 on clones sampled at 8, 10, 12, and 14 h post-infection revealed a progressive
390 shift from susceptible to resistant phenotypes, supporting the model's prediction that the resistant
391 subpopulation emerged and start to proliferate around 8 hours after infection onset.

392 Additional evidence supporting the presence of coexisting subpopulations during the kinetics comes from the
393 observation that, in certain phage–bacterium pairs (e.g., V1SA019 and SH1000), the phage concentration does
394 not simply reach a peak and remain stable, but instead shows a slight decline after 10 hours (by 0.5 to 1 $\log_{10}$).
395 This pattern, previously reported by Cairns *et al.* in a different phage–bacterium system [5], suggests a potentially
396 generalizable phenomenon rather than an experimental artifact. One possible explanation is that phages may
397 acquire mutations enabling them to infect the resistant bacterial population [29], [30]. An alternative explanation
398 could involve the coexistence of phages with both susceptible and resistant bacterial subpopulations over time
399 [31], [32]. These findings underscore the need for future studies to monitor the proportions of susceptible and
400 resistant bacteria throughout the experiment and to perform sequencing of both bacterial and phage
401 populations to detect the possible emergence of mutant lineages.

402

403 **Conclusion**

404 Our mechanistic PK/PD model reliably captures the complex dynamics of phage – *S. aureus* interactions, including
405 resistance emergence. Its relevance now warrants evaluation using *in vivo* data to support translational
406 applicability.

Acknowledgments

The authors acknowledge the scientific review service of Hospices Civils de Lyon for the English writing proofreading.

This study was supported by the French Agence Nationale pour la Recherche (PHAG-ONE project, ANR 20-PAMR-0009).

Supplementary Materials and Methods

Adsorption time assay and One-Step Growth Curve experiment (burst size)

Adsorption time is the time required for bacteriophage to be absorbed into host bacterial cells as first stage of phage infection. Adsorption time was set as the time required for 95% of the phage population to be attached to a bacterium. Phage adsorption tests were performed as described by Marashi and colleagues with few modifications [33]. Briefly, phages were added to late log phase cultures of SH1000 or USA300 strains in 25 mL of caMH in a 50 mL conical tubes (approximately 10^8 CFU mL^{-1}) at an approximate MOI of 0.01 and incubated at 37°C without agitation. Samples were taken every 4 min up to 45 min after phage addition and were passed through a 0.2 µm filter (Merk, Darmstadt, Germany) to remove *S. aureus* cells and bound phages. Unbound 'free' phages were counted using spot tests and double layer plaque assays. To estimate the latent period (which is defined as the time between absorption and the beginning of the first burst) and burst size (which is defined as the number of new phages produced and released by an infected bacterium) of a single round of phage replication, the same protocol was applied with modifications: culture was serial diluted in pre-warmed caMH at 1/100, 1/1000 and 1/10000 at "T= Adsorption time" according to Kropinski and colleagues [34]. Samples were taken every 6 min up to 2 h post phage addition. The data obtained from the most diluted flask were used during analyses to avoid re-adsorption phenomena. The burst size value was calculated as follows: "Average phage concentration at plateau/Number of adsorbed phages at T= Adsorption time" [34]. The one-step growth curve experiment was carried out in triplicates using three phage production batches.

[1] J. A. G. Fortaleza, C. J. N. Ong, and R. De Jesus, 'Efficacy and clinical potential of phage therapy in treating methicillin-resistant Staphylococcus aureus (MRSA) infections: A review', *Eur J Microbiol Immunol (Bp)*, Feb. 2024, doi: 10.1556/1886.2023.00064.

[2] M. T. Moghadam *et al.*, 'Phage therapy as a glimmer of hope in the fight against the recurrence or emergence of surgical site bacterial infections', *Infection*, Feb. 2024, doi: 10.1007/s15010-024-02178-0.

[3] D. M. Lin, B. Koskella, and H. C. Lin, 'Phage therapy: An alternative to antibiotics in the age of multi-drug resistance', *World J Gastrointest Pharmacol Ther*, vol. 8, no. 3, pp. 162–173, Aug. 2017, doi: 10.4292/wjgpt.v8.i3.162.

[4] S. C. Nang *et al.*, 'Pharmacokinetics/pharmacodynamics of phage therapy: a major hurdle to clinical translation', *Clin Microbiol Infect*, vol. 29, no. 6, pp. 702–709, Jun. 2023, doi: 10.1016/j.cmi.2023.01.021.

[5] B. J. Cairns, A. R. Timms, V. A. A. Jansen, I. F. Connerton, and R. J. H. Payne, 'Quantitative models of in vitro bacteriophage-host dynamics and their application to phage therapy', *PLoS Pathog*, vol. 5, no. 1, p. e1000253, Jan. 2009, doi: 10.1371/journal.ppat.1000253.

[6] 'Staphylococcus aureus in Healthcare Settings | HAI | CDC'. Accessed: Feb. 12, 2024. [Online]. Available: https://www.cdc.gov/hai/organisms/staph.html

[7] 'WHO publishes list of bacteria for which new antibiotics are urgently needed'. Accessed: Nov. 15, 2023. [Online]. Available: https://www.who.int/news/item/27-02-2017-who-publishes-list-of-bacteria-for-which-new-antibiotics-are-urgently-needed

[8] M. J. Horsburgh, J. L. Aish, I. J. White, L. Shaw, J. K. Lithgow, and S. J. Foster, 'sigmaB modulates virulence determinant expression and stress resistance: characterization of a functional rsbU strain derived from Staphylococcus aureus 8325-4', *J Bacteriol*, vol. 184, no. 19, pp. 5457–5467, Oct. 2002, doi: 10.1128/JB.184.19.5457-5467.2002.

[9] B. A. Diep *et al.*, 'Complete genome sequence of USA300, an epidemic clone of community-acquired meticillin-resistant Staphylococcus aureus', *Lancet*, vol. 367, no. 9512, pp. 731–739, Mar. 2006, doi: 10.1016/S0140-6736(06)68231-7.

[10] C. Kolenda *et al.*, 'Phage Therapy against Staphylococcus aureus: Selection and Optimization of Production Protocols of Novel Broad-Spectrum Silviavirus Phages', *Pharmaceutics*, vol. 14, no. 9, p. 1885, Sep. 2022, doi: 10.3390/pharmaceutics14091885.

[11] 'Double-Layer Plaque Assay Technique for Enumeration of Virus Surrogates | Springer Nature Experiments'. Accessed: May 19, 2025. [Online]. Available: https://experiments.springernature.com/articles/10.1007/978-1-0716-1932-2_14

[12] D. Chae, 'Phage-host-immune system dynamics in bacteriophage therapy: basic principles and mathematical models', *Transl Clin Pharmacol*, vol. 31, no. 4, pp. 167–190, Dec. 2023, doi: 10.12793/tcp.2023.31.e17.

[13] A. Bankevich *et al.*, 'SPAdes: A New Genome Assembly Algorithm and Its Applications to Single-Cell Sequencing', *J Comput Biol*, vol. 19, no. 5, pp. 455–477, May 2012, doi: 10.1089/cmb.2012.0021.

[14] O. Schwengers, L. Jelonek, M. A. Dieckmann, S. Beyvers, J. Blom, and A. Goesmann, 'Bakta: rapid and standardized annotation of bacterial genomes via alignment-free sequence identification', *Microb Genom*, vol. 7, no. 11, p. 000685, Nov. 2021, doi: 10.1099/mgen.0.000685.

[15] G. Marçais, A. L. Delcher, A. M. Phillippy, R. Coston, S. L. Salzberg, and A. Zimin, 'MUMmer4: A fast and versatile genome alignment system', *PLoS Comput Biol*, vol. 14, no. 1, p. e1005944, Jan. 2018, doi: 10.1371/journal.pcbi.1005944.

[16] R. J. Payne, D. Phil, and V. A. Jansen, 'Phage therapy: the peculiar kinetics of self-replicating pharmaceuticals', *Clin Pharmacol Ther*, vol. 68, no. 3, pp. 225–230, Sep. 2000, doi: 10.1067/mcp.2000.109520.

[17] R. J. H. Payne and V. A. A. Jansen, 'Pharmacokinetic principles of bacteriophage therapy', *Clin Pharmacokinet*, vol. 42, no. 4, pp. 315–325, 2003, doi: 10.2165/00003088-200342040-00002.

[18] C. Y. (Joey) Leung and J. S. Weitz, 'Modeling the synergistic elimination of bacteria by phage and the innate immune system', *Journal of Theoretical Biology*, vol. 429, pp. 241–252, Sep. 2017, doi: 10.1016/j.jtbi.2017.06.037.

[19] T. Bigwood, J. A. Hudson, and C. Billington, 'Influence of host and bacteriophage concentrations on the inactivation of food-borne pathogenic bacteria by two phages', *FEMS Microbiol Lett*, vol. 291, no. 1, pp. 59–64, Feb. 2009, doi: 10.1111/j.1574-6968.2008.01435.x.

[20] J. M. Obeso, P. García, B. Martínez, F. N. Arroyo-López, A. Garrido-Fernández, and A. Rodriguez, 'Use of Logistic Regression for Prediction of the Fate of Staphylococcus aureus in Pasteurized Milk in the Presence of Two Lytic Phages', *Applied and Environmental Microbiology*, vol. 76, no. 18, pp. 6038–6046, Sep. 2010, doi: 10.1128/AEM.00613-10.

[21] R. J. Payne and V. A. Jansen, 'Understanding bacteriophage therapy as a density-dependent kinetic process', *J Theor Biol*, vol. 208, no. 1, pp. 37–48, Jan. 2001, doi: 10.1006/jtbi.2000.2198.
[22] A. A. Schmalstig, S. Freidy, P. O. Hanafin, M. Braunstein, and G. G. Rao, 'Reapproaching Old Treatments: Considerations for PK/PD Studies on Phage Therapy for Bacterial Respiratory Infections', *Clin Pharmacol Ther*, vol. 109, no. 6, pp. 1443–1456, Jun. 2021, doi: 10.1002/cpt.2214.
[23] L. M. Kasman, A. Kasman, C. Westwater, J. Dolan, M. G. Schmidt, and J. S. Norris, 'Overcoming the Phage Replication Threshold: a Mathematical Model with Implications for Phage Therapy', *J Virol*, vol. 76, no. 11, pp. 5557–5564, Jun. 2002, doi: 10.1128/JVI.76.11.5557-5564.2002.
[24] S. T. Abedon, 'Phage therapy dosing: The problem(s) with multiplicity of infection (MOI)', *Bacteriophage*, vol. 6, no. 3, p. e1220348, Aug. 2016, doi: 10.1080/21597081.2016.1220348.
[25] A. Leprince and J. Mahillon, 'Phage Adsorption to Gram-Positive Bacteria', *Viruses*, vol. 15, no. 1, p. 196, Jan. 2023, doi: 10.3390/v15010196.
[26] J. Bertozzi Silva, Z. Storms, and D. Sauvageau, 'Host receptors for bacteriophage adsorption', *FEMS Microbiol Lett*, vol. 363, no. 4, p. fnw002, Feb. 2016, doi: 10.1093/femsle/fnw002.
[27] S. M. Lehman *et al.*, 'Design and Preclinical Development of a Phage Product for the Treatment of Antibiotic-Resistant Staphylococcus aureus Infections', *Viruses*, vol. 11, no. 1, Art. no. 1, Jan. 2019, doi: 10.3390/v11010088.
[28] R. Capparelli, M. Parlato, G. Borriello, P. Salvatore, and D. Iannelli, 'Experimental Phage Therapy against Staphylococcus aureus in Mice', *Antimicrobial Agents and Chemotherapy*, vol. 51, no. 8, pp. 2765–2773, Aug. 2007, doi: 10.1128/aac.01513-06.
[29] B. R. Levin and J. J. Bull, 'Population and evolutionary dynamics of phage therapy', *Nat Rev Microbiol*, vol. 2, no. 2, pp. 166–173, Feb. 2004, doi: 10.1038/nrmicro822.
[30] D. T. Kysela and P. E. Turner, 'Optimal bacteriophage mutation rates for phage therapy', *J Theor Biol*, vol. 249, no. 3, pp. 411–421, Dec. 2007, doi: 10.1016/j.jtbi.2007.08.007.
[31] A. Rabinovitch, I. Aviram, and A. Zaritsky, 'Bacterial debris-an ecological mechanism for coexistence of bacteria and their viruses', *J Theor Biol*, vol. 224, no. 3, pp. 377–383, Oct. 2003, doi: 10.1016/s0022-5193(03)00174-7.
[32] 'Alternative stable states in host–phage dynamics | Theoretical Ecology'. Accessed: Feb. 27, 2024. [Online]. Available: https://link.springer.com/article/10.1007/s12080-007-0001-1
[33] S. M. A. Marashi, F. Nikkhahi, D. Hamedi, and G. Shahbazi, 'Isolation, Characterization and in vitro Evaluation of Specific Bacteriophages Targeting Extensive Drug Resistance Strains of Pseudomonas aeruginosa Isolated from Septic Burn Wounds', *Infection & Chemotherapy*, vol. 54, no. 1, pp. 153–164, Mar. 2022, doi: 10.3947/ic.2021.0132.
[34] A. M. Kropinski, 'Practical Advice on the One-Step Growth Curve', *Methods Mol Biol*, vol. 1681, pp. 41–47, 2018, doi: 10.1007/978-1-4939-7343-9_3.

526 **Table 1**. Parameter estimates of the phage-bacteria co-dynamics for *S. aureus* SH1000 / V1SA019

	Parameter	Value	Relative standard error (%)	Bootstrap estimates		
				P2.5	Median	P97.5
Fixed effects[a]	1. alpha (h^{-1})	1.64	1.91	1.45	1.62	1.70
	2. Bmax (CFU/mL)	1.32E+10	NA (fixed)	NA	NA	NA
	3. mut (h^{-1})	2.64E-09	44.2	6.97E-10	2.56E-09	1.25E-08
	4. $bind_S$ (h^{-1})	2.45E-09	8.6	1.34E-09	2.30E-09	3.31E-09
	5. $bind_R$ (h^{-1})	4.47E-11	7.6	1.94E-11	3.86E-11	5.75E-11
	6. lysis (h^{-1})	6.98	9.9	5.53343	7.16135	9.64491
	7. burst (PFU/mL)	179	22.4	102.83	203.832	692.648
	8. decay (h^{-1})	0.0177	13.6	0.0111	0.0186	0.0248
Random effects[b]	9. omega_alpha	0.043 (4.3 %)	35.2	0.017	0.034	0.117
	10. omega_mut	1.49 (286 %)	29.1	0.75	1.45	2.28
	11. omega_$bind_S$	0.335 (34 %)	48.6	0.126	0.368	0.823
	12. omega_$bind_R$	0.151 (15 %)	43.0	0.0995	0.231	0.686
	13. omega_lysis	0.398 (41 %)	17.8	0.274	0.409	0.564
	14. omega_burst	0.861 (105 %)	17.5	0.471	0.893	1.262
	15. omega_dec	0.442 (46 %)	28.6	0.193	0.369	0.651
Error model parameters[c]	16. a(B)	0.548 (4.52 %)	4.52	0.476	0.546	0.622
	17. a(V)	0.11 (14.3 %)	14.3	0.059	0.107	0.173
	18. b(V)	0.0553 (6.61 %)	6.61	0.0345	0.0537	0.0680
Others[d]	19. $Prolif_S$ (CFU/mL)	4.8E+04 (54.8 %)	NA	NA	NA	NA
	20. $Inund_S$ (PFU/mL)	6.8E+08 (14.6 %)	NA	NA	NA	NA
	21. $Prolif_R$ (CFU/mL)	2.67E+06 (69.1 %)	NA	NA	NA	NA
	22. $Inund_R$ (PFU/mL)	3.68E+10 (3.3 %)	NA	NA	NA	NA

527

528 [a] Fixed effect parameters are as described in the main text.

529 [b] Omega parameters are expressed as standard deviations of random effects along with coefficient of variation

530 of the corresponding parameter within brackets

[c] Error model parameters are as follows: a(B), coefficient of additive error of bacteria count, a(V) and b(V), coefficient of additive and proportional error of phage count, respectively.

[d] Proliferation and inundation threshold values are given as mean (CV %) of Bayesian posterior estimates from each experiment.

1 to 22: Line number.

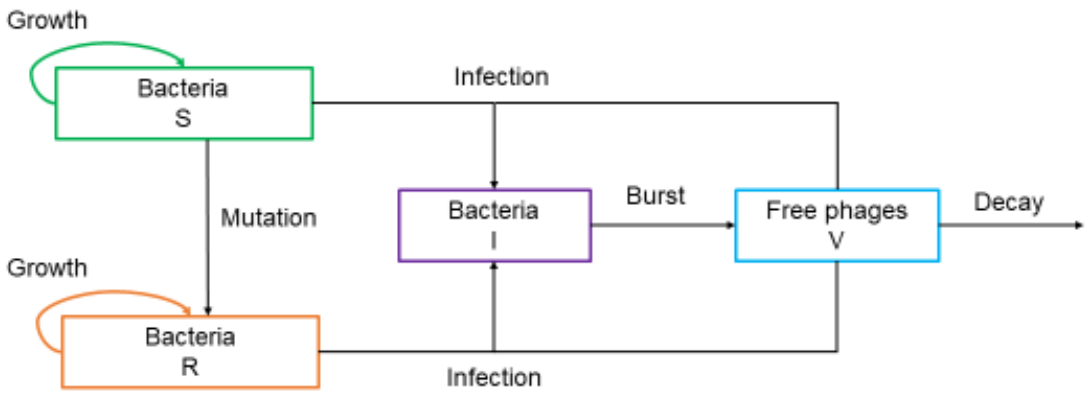

Figure 1. Structural model of the bacteria – phage co-dynamics

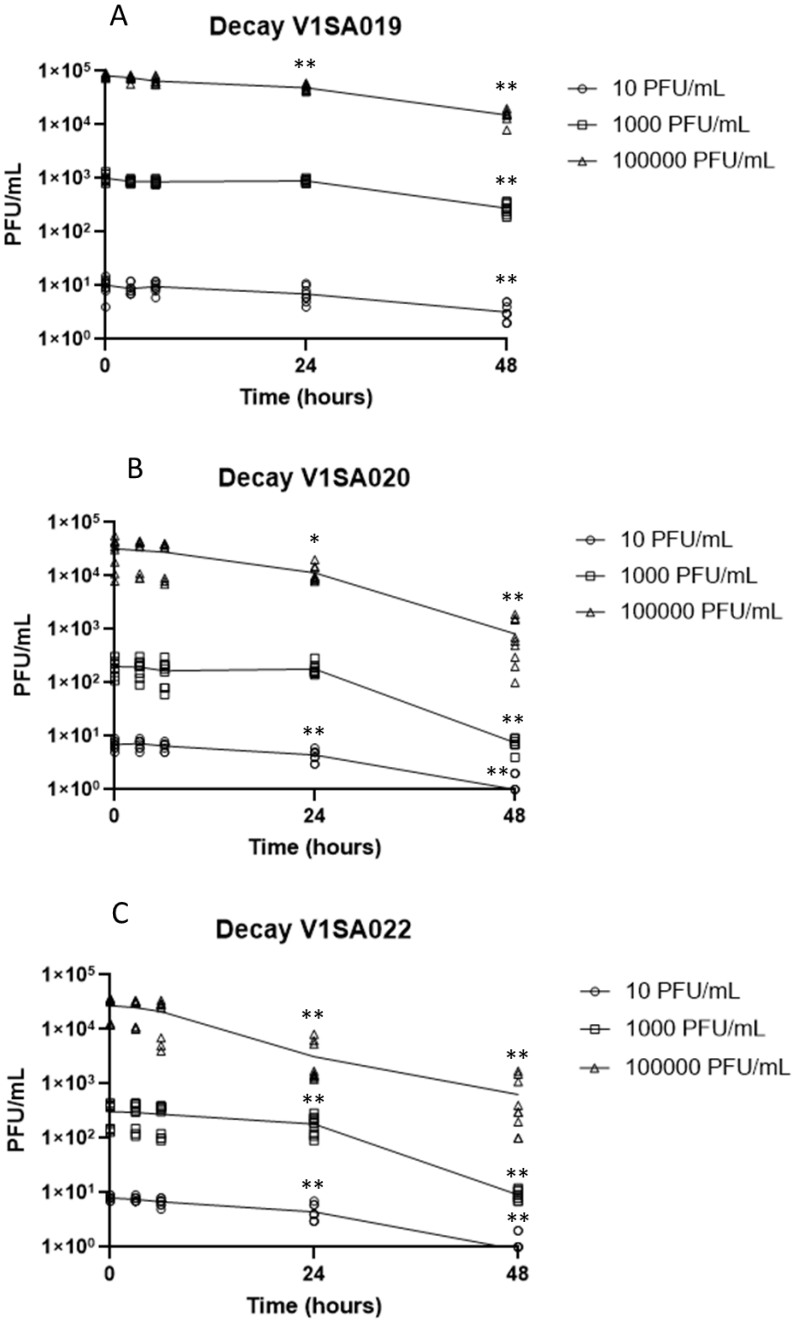

Figure 2. Phage decay of V1SA019 (A), V1SA020 (B), V1SA022 (C). Each symbol represents an experimental point. Connecting line represents the median. Statistical analysis compared two time points via Wilcoxon matched pairs signed rank test. *: p-value < 0.05 ; **: p-value < 0.005.

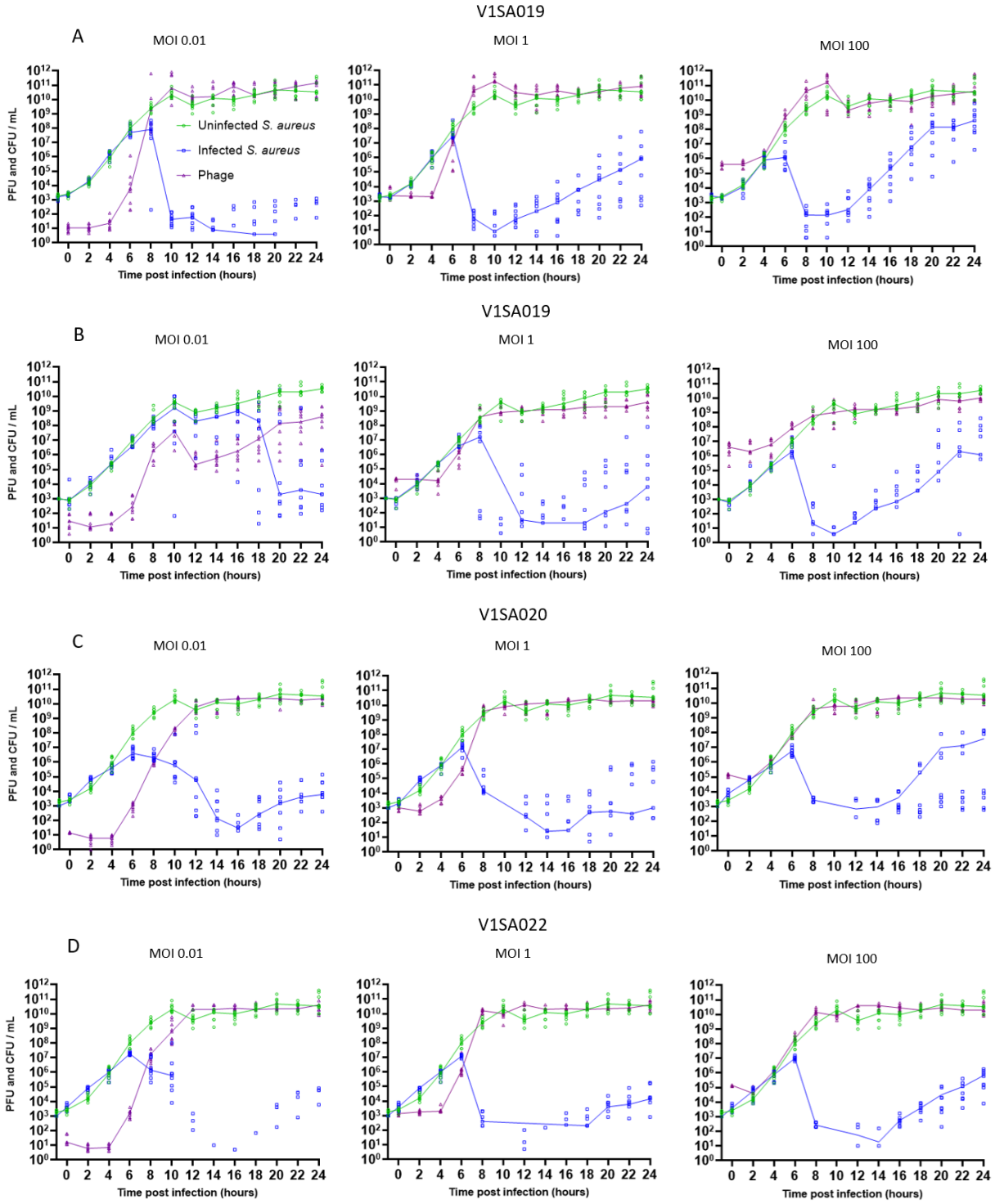

Figure 3. *in vitro* time-kill experiments between V1SA019 and SH1000(A) or USA300 (B), V1SA020 and SH1000 (C), V1SA022 and SH1000 (D). Each symbol represents an experimental point. Connecting line represents the median. Green: Enumeration of S. *aureus* in absence of phage (control condition). Blue: Enumeration of S. *aureus* in the presence of phage. Purple: Free phages in the presence of S. *aureus*.

564 **A**

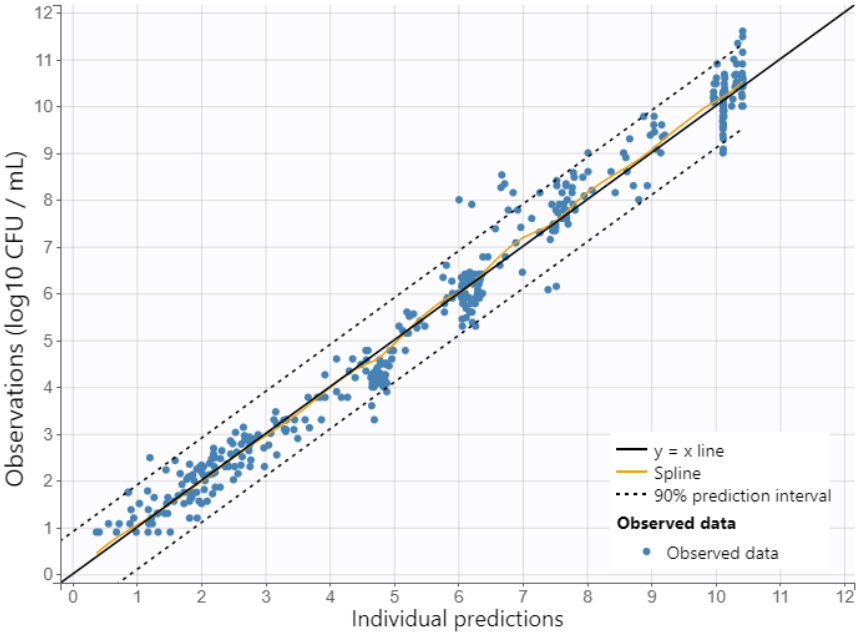

565

566 **B**

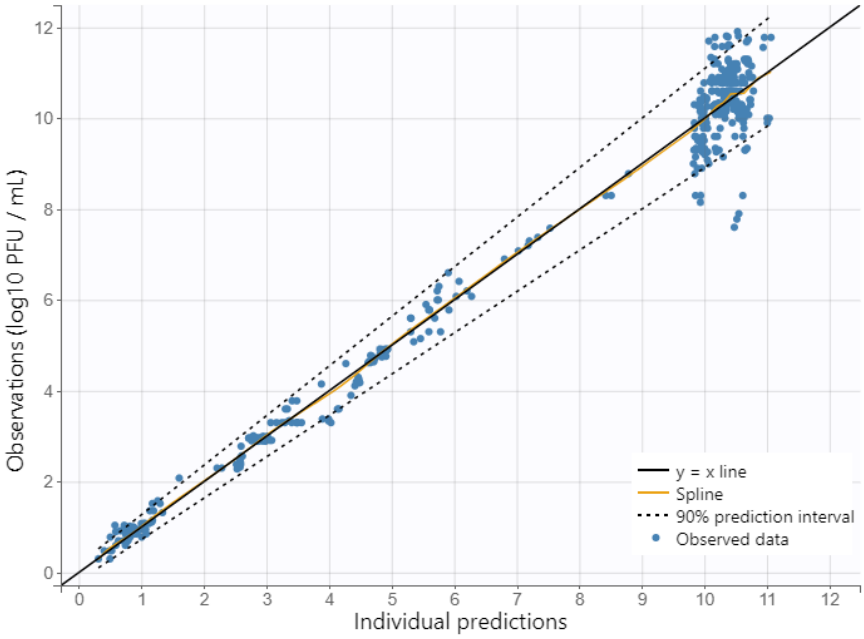

567

568 **Figure 4. Observations versus model-based predictions of bacteria (A) and phage (B) counts for the V1SA019 /**
569 **SH1000 pair.**
570 The blue dots indicate observation-prediction pairs. The black solid line is the y = x line, the yellow line is the

571 spline regression line. The dashed lines indicate the 90 % prediction interval.

572

573 A

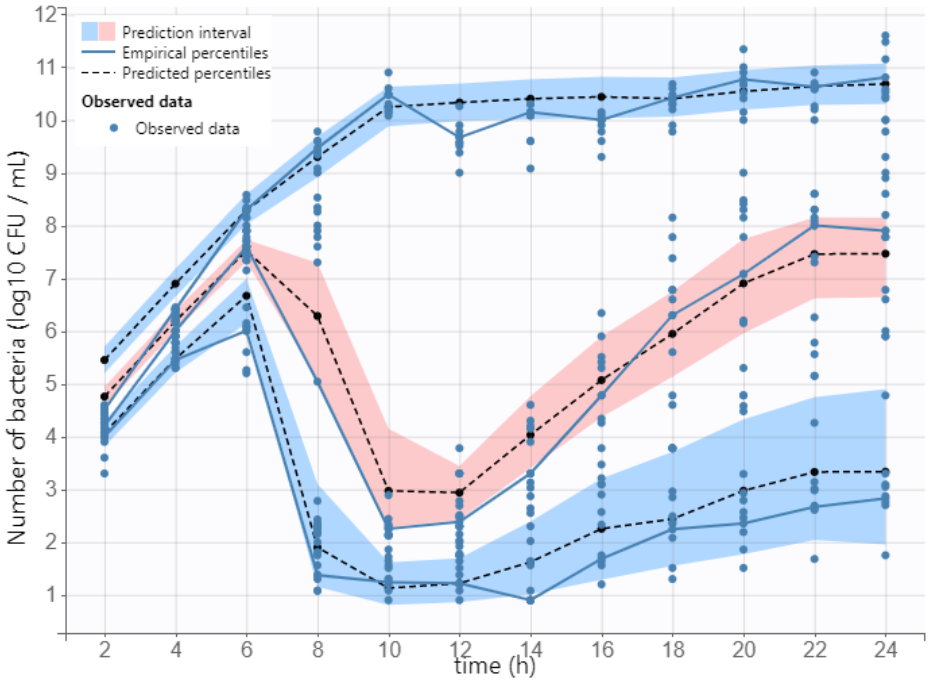

574

575 B

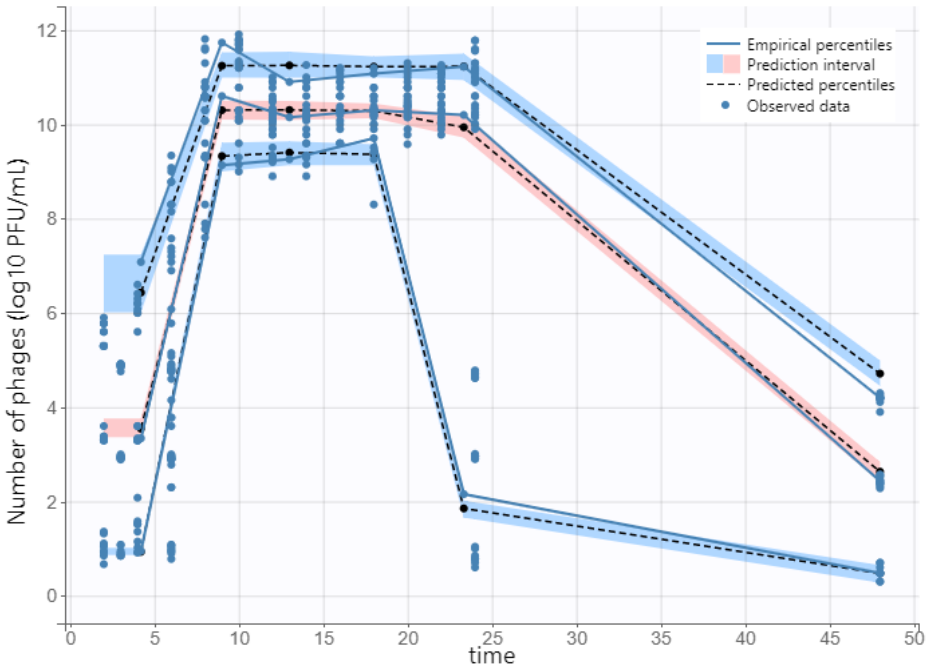

576

577 **Figure 5. Visual predictive checks obtained with the final model for the V1SA019 / SH1000 pair.** A and B panels
578 show VPC for bacteria and phage, respectively. Blue dots are observed data. Blue solid and black dashed lines
579 are 10th, 50th (median) and 90th percentiles of observed and simulated data (n = 1000 for each experiment),
580 respectively. Blue and pink colored areas are 90 % prediction intervals of corresponding simulated percentiles.

581

A

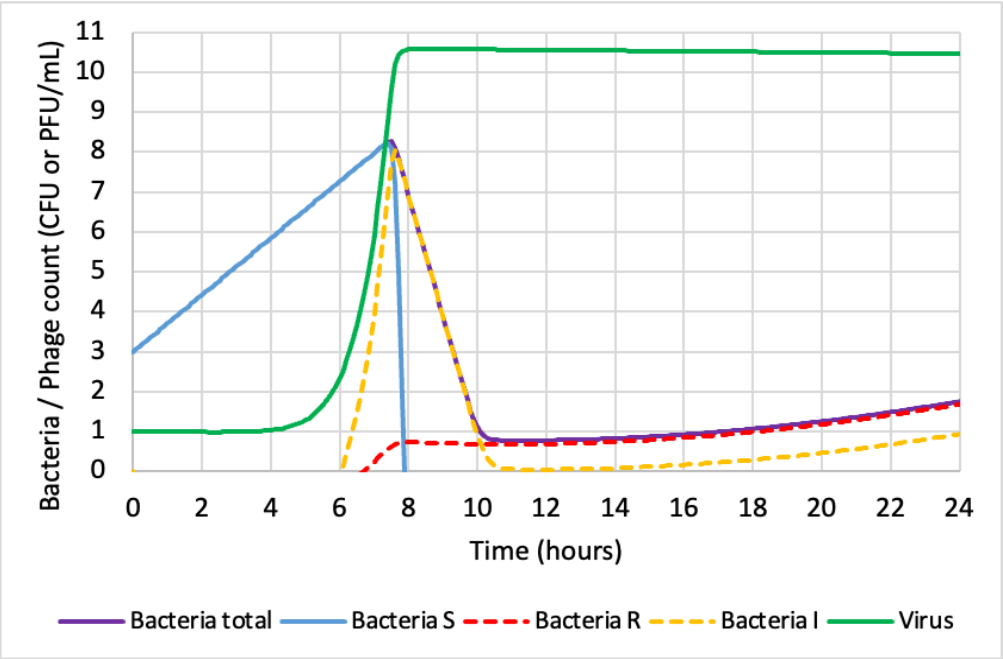
Bacteria / Phage count (CFU or PFU/mL)
11
10
9
8
7
6
5
4
3
2
1
0
0
2
4
6
8
10
12
14
16
18
20
22
24
Time (hours)
Bacteria total
Bacteria S
Bacteria R
Bacteria I
Virus

B

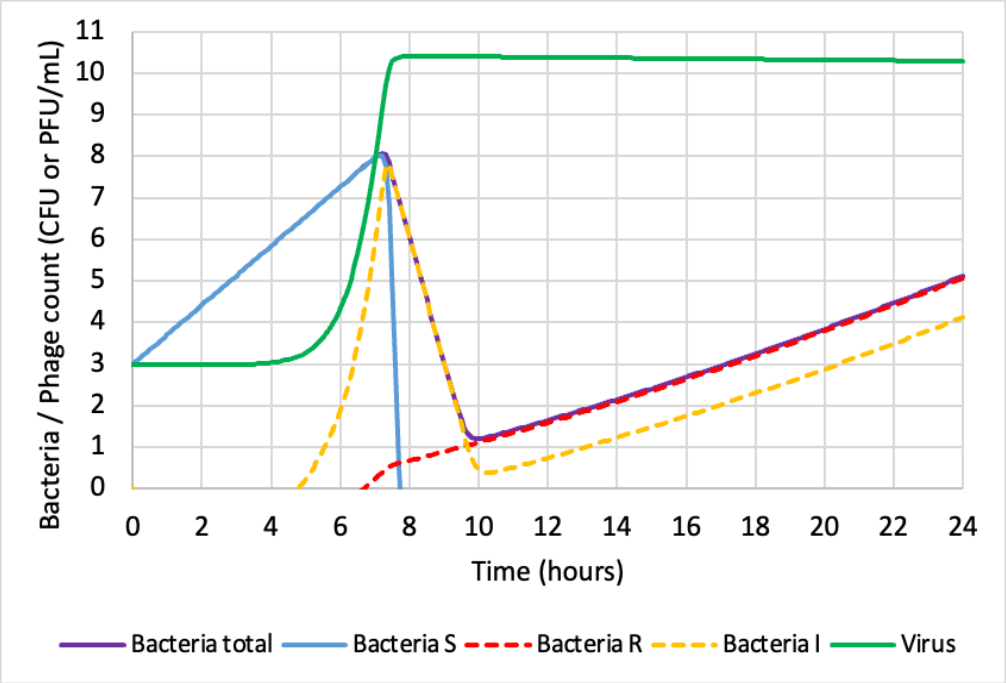
Bacteria / Phage count (CFU or PFU/mL)
11
10
9
8
7
6
5
4
3
2
1
0
0
2
4
6
8
10
12
14
16
18
20
22
24
Time (hours)
Bacteria total
Bacteria S
Bacteria R
Bacteria I
Virus

587 C

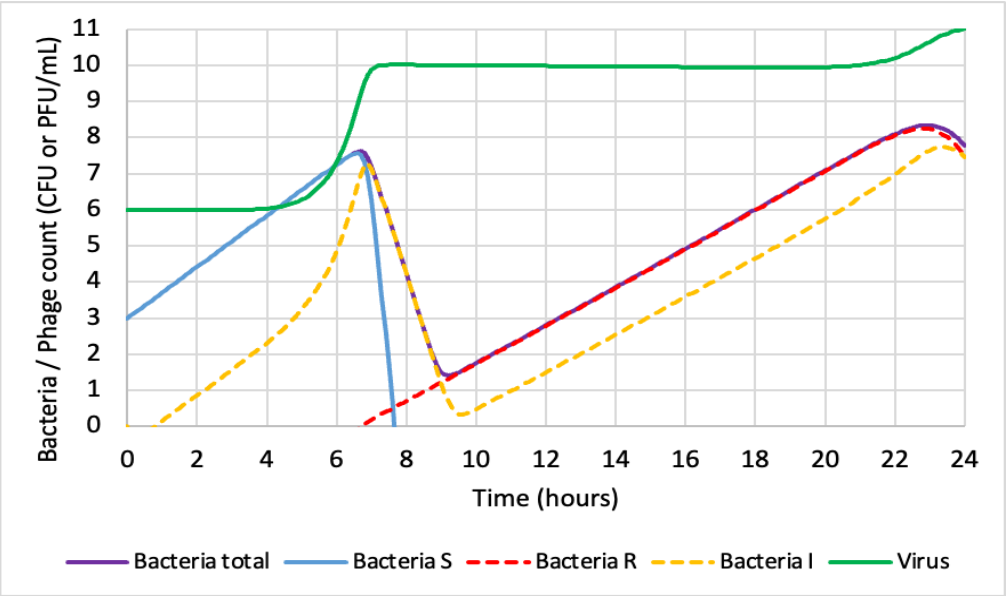

588

589 D

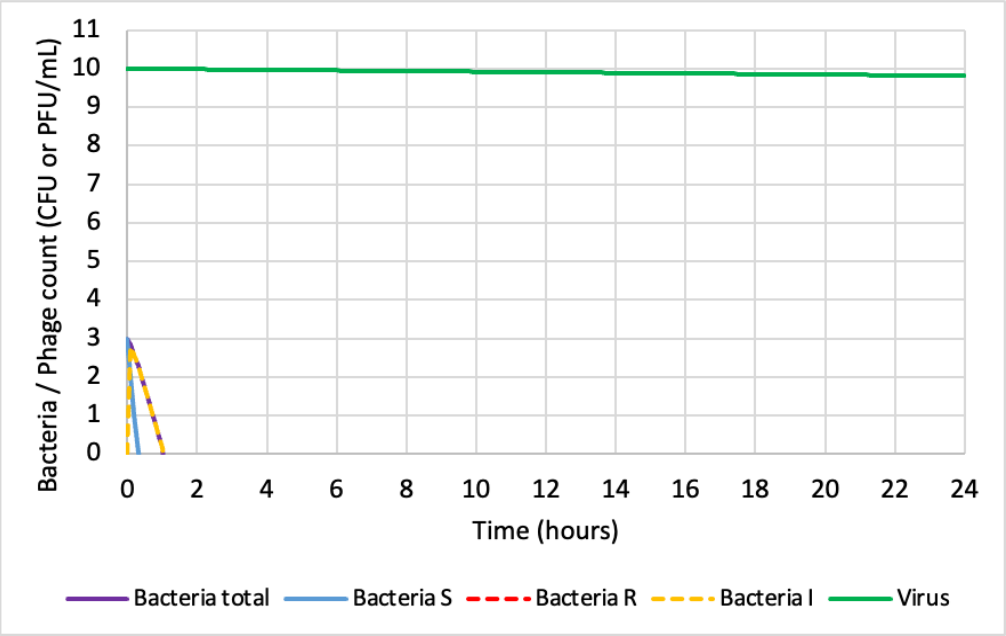

590

591 **Figure 6. Simulated dynamics of bacteria and phage**

592 Simulations were performed with typical parameter values of the final model for V1SA019 / SH1000 reported in

593 . Initial number of susceptible bacteria is 10^3 in all simulations. Initial number of phages is 10, 10^3, 10^6 and 10^{10}
594 in panel A, B, C, and D, respectively.

595

596 **Supplementary Table S1. Adsorption time** determined for phages V1SA019, V1SA020, V1SA022 on strains
597 SH1000 and USA300. nd: not determined. Adsorption time is defined as the time where 95% of phages are
598 adsorbed on bacteria.

Adsorption time (min)		Bacterial strains	
		SH1000	**USA300**
Phages	**V1SA019**	8	12
	V1SA020	28	nd
	V1SA022	24	nd

599

600 **Supplementary Table S2. Burst size values** determined for phages V1SA019, V1SA020, V1SA022 on strains
601 SH1000 and USA300. Calculation based on data from One-Step Growth Curve experiment. nd: not determined.

Burst size values		Bacterial strains	
		SH1000	**USA300**
Phages	**V1SA019**	42	134
	V1SA020	24	nd
	V1SA022	27	nd

602

603 **Supplementary Table S3. Comparison of parameters of the phage-bacteria co-dynamics for the 4**
604 **bacteria/phage pairs.**

605

	Parameter	**SH1000 / V1SA019**	**SH1000 / V1SA020**	**SH1000 / V1SA022**	**USA300 / V1SA019**
Fixed effects[a]	1. alpha (h^{-1})	1.64 (1.91 %)	1.33 (3.92 %)	1.31 (3.29 %)	1.8 (2.66 %)
	2. Bmax (CFU/mL)	1.32E+10 (NA, fixed)	1.9E+10 (43.7 %)	2.72E+10 (30.9 %)	5.23e+08 (32.5 %)
	3. mut (h^{-1})	2.64E-09 (44.2 %)	1.46E-10 (382 %)	6.85E-13 (>200 %)	1.26e-13 (>200 %)
	4. $bind_S$ (h^{-1})	2.45E-09 (8.6 %)	6.19e-09 (22 %)	2.74E-09 (21.2 %)	1.7e-08 (12.6 %)
	5. $bind_R$ (h^{-1})	4.47E-11 (7.6 %)	5.65e-11 (14.6 %)	1.09E-11 (42.4 %)	4.82e-10 (33.5 %)
	6. lysis (h^{-1})	6.98 59.9 %)	4.37 (8.13 %)	5.96 (13.6 %)	6.29 (12.7 %)
	7. burst (PFU/mL)	179 (22.4 %)	139 (45.6 %)	503 (35 %)	17.9 (33.9 %)
	8. decay (h^{-1})	0.0177 (13.6 %)	0.0336 (18.6 %)	0.0499 (16.7 %)	0.0109 (45.7 %)
Random effects[b]	9. omega_alpha	0.043 (35.2 %)	0.207 (11.8 %)	0.172 (11.6 %)	0.108 (24.8 %)
	10. Omega_Bmax	NA	0.82 (40.2 %)	0.754 (32 %)	1.63 (14 %)

	Parameter	SH1000 / V1SA019	SH1000 / V1SA020	SH1000 / V1SA022	USA300 / V1SA019
	11. omega_mut	1.49 (29.1 %)	2.57 (46.8 %)	4.59 (28.4 %)	7.62 (29.7 %)
	12. omega_bind$_S$	0.335 (48.6 %)	1.17 (15.8 %)	1.35 (14.5 %)	0.604 (18.4 %)
	13. omega_bind$_R$	0.151 (43.0 %)	0.243 (27.9 %)	0.745 (38.2 %)	0.962 (33.1 %)
	14. omega_lysis	0.398 (17.8 %)	0.427 (15.1 %)	0.634 (17.6 %)	0.599 (27 %)
	15. omega_burst	0.861 (17.5 %)	0.963 (17.1 %)	1.25 (21.9 %)	1.48 (13.8 %)
	16. omega_dec	0.442 (28.6 %)	0.53 (29.1 %)	0.492 (33 %)	1.41 (21.5 %)
Error model parameters[c]	17. a(B)	0.548	0.6	0.575	0.824
	18. a(V)	0.11	0.38	0.319	0.168
	19. b(V)	0.0553	NA	NA	0.0475
Others[d]	20. Prolif$_S$ (CFU/mL)	4.8E+04 (54.8 %)	7.00E+04 (174.9 %)	4.78E+04 (63.8 %)	2.12E+05 (350.5 %)
	21. Inund$_S$ (PFU/mL)	6.8E+08 (14.6 %)	2.95E+08 (74.7 %)	6.21E+08 (64.5 %)	1.11E+08 (36.5 %)
	22. Prolif$_R$ (CFU/mL)	2.67E+06 (69.1 %)	6.19E+06 (121.7 %)	1.50E+07 (173.7 %)	9.64E+06 (598.4 %)
	23. Inund$_R$ (PFU/mL)	3.68E+10 (3.3 %)	2.40E+10 (18.1 %)	1.19E+11 (24.7 %)	3.76E+09 (33.1 %)

[a] Fixed effect parameters are as described in the main text and expressed as population estimate (relative standard error).

[b] Omega parameters are expressed as standard deviations of random effects (relative standard errors)

[c] Error model parameters are as follows: a(B), coefficient of additive error of bacteria count, a(V) and b(V), coefficient of additive and proportional error of phage count, respectively.

[d] Proliferation and inundation threshold values are given as mean (CV %) of Bayesian posterior estimates from each experiment.

1 to 23: Line number

616 **Supplementary Table S4. List of mutated genes in SH1000** after 24 h of exposure to phage V1SA019. In bold:
617 genes involved in the teichoic acid biosynthesis pathway.

618

MOI	Mutant	Gene	Effect
0.01	KR19	**tarK**	missense_variant c.536A>G p.His179Arg
		tarA	missense_variant c.665G>T p.Arg222Ile
		purR	missense_variant c.286C>T p.Arg96Cys
	KR20	S35	intragenic_variant n.508155A>G
		tarK	missense_variant c.536A>G p.His179Arg
		tsr24	non_coding_transcript_variant
		tarA	missense_variant c.665G>T p.Arg222Ile
		znuB	missense_variant c.143G>A p.Ser48Asn
	KR21	tsr24	non_coding_transcript_variant
		tarA	missense_variant c.665G>T p.Arg222Ile
1	KR25	tsr24	non_coding_transcript_variant
		rpoB	missense_variant c.2161A>G p.Thr721Ala
		rfe/tagO	frameshift_variant&missense_variant c.556delGinsAT p.Val186fs
	KR26	S35	intragenic_variant n.508155A>G
		tsr24	non_coding_transcript_variant
		mrcB	disruptive_inframe_insertion c.785_787dupGCA p.Arg262_Ile263insSer
		tarA	missense_variant c.665G>T p.Arg222Ile
	KR27	mrcB	missense_variant c.691C>T p.Pro231Ser
		tarA	missense_variant c.665G>T p.Arg222Ile
100	KR31	**rfe/tagO**	deletion of 823 nucleotides
	KR32	**tarK**	missense_variant c.536A>G p.His179Arg
		rfe/tagO	frameshift_variant c.853delG p.Val285fs
	KR33	**tarK**	missense_variant c.536A>G p.His179Arg
		rfe/tagO	frameshift_variant c.853delG p.Val285fs

619

620

621 **Supplementary Table S5. Apparition of SH1000 resistant mutants to V1SA019** over time of kinetic according to
622 MOI. nd: not determined.

Resistants to V1SA019 (total tested)		**Time of kinetic**				
		8 h	**10 h**	**12 h**	**14 h**	**24 h**
MOI	**0.01**	0 (30)	0 (30)	0 (30)	1 (3)	23 (24)
	1	1 (15)	0 (15)	0 (22)	10 (10)	30 (30)
	100	2 (30)	5 (27)	nd	nd	30 (30)

623

624

625

626

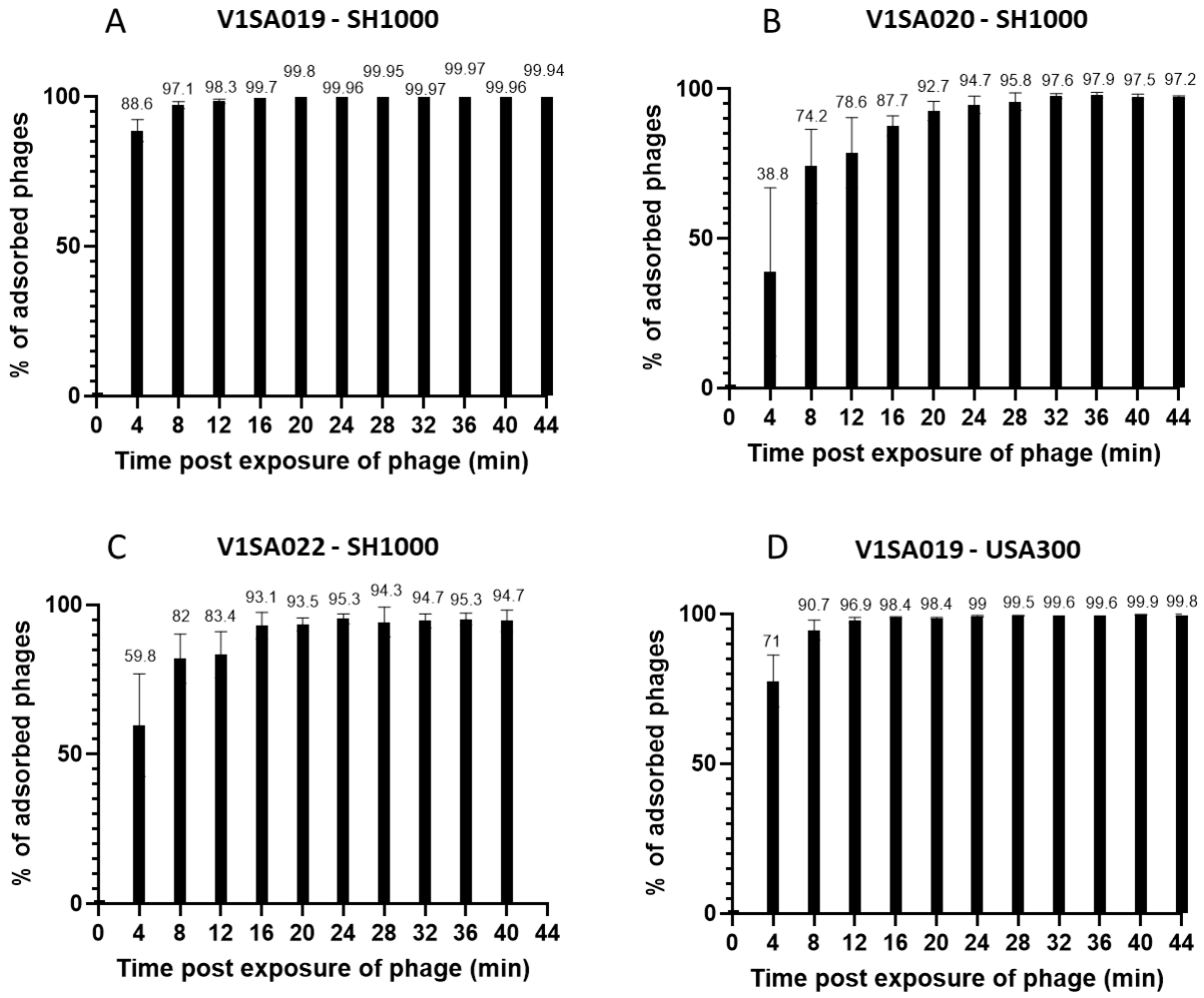

Supplementary Figure S1. Adsorption kinetics for V1SA019 (A), V1SA020 (B), V1SA022 (C) phages on SH1000 strain and V1SA019 (D) on USA300 strain. Each graph represents the average of 3 independent experiments with standard deviation. The percentage of phage adsorption is indicated at the top of each column.

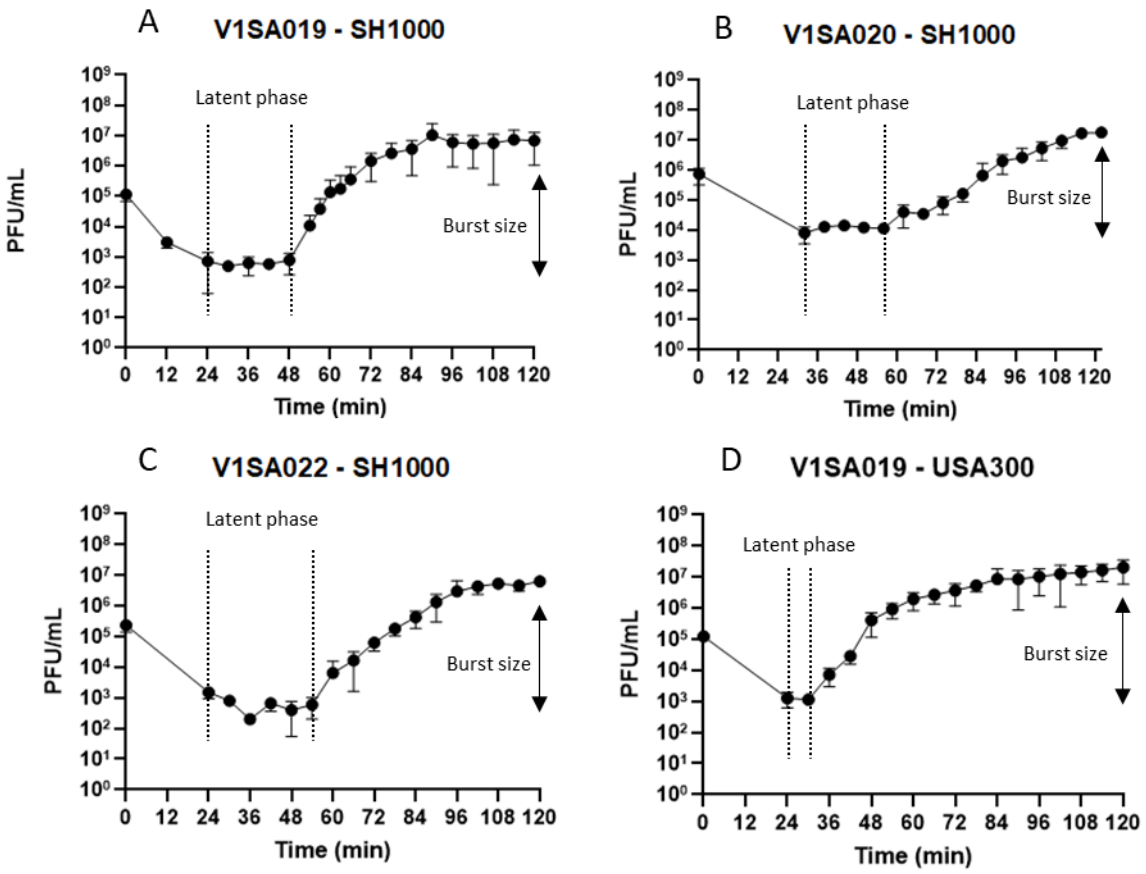

Supplementary Figure S2. One-Step Growth Curve (for burst size value calculation) for V1SA019 (A), V1SA020 (B), V1SA022 (C) phages on SH1000 strain and V1SA019 (D) on USA300 strain. Each circle represents the average of 3 independent experiments with standard deviation. The latent phase is indicated between the dotted lines. The solid arrow represents the burst size.

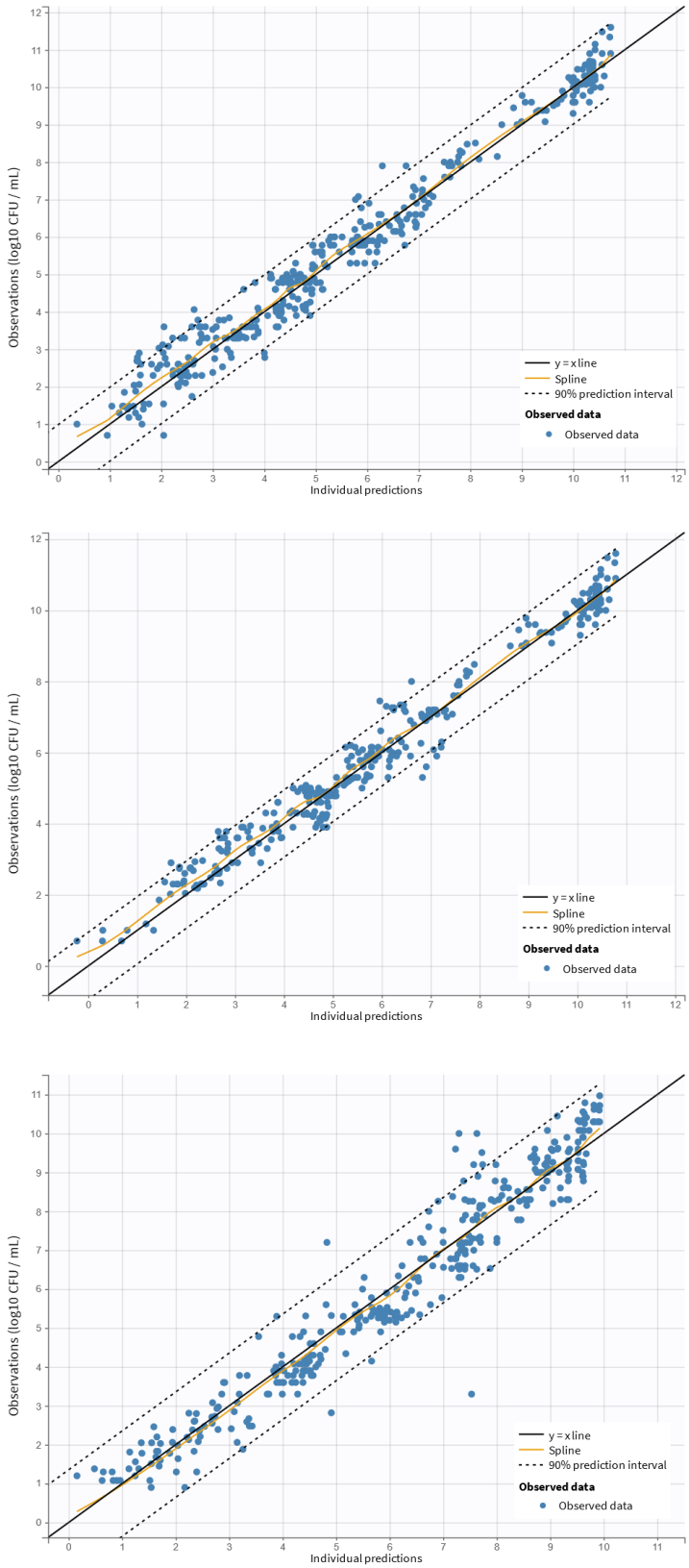

Supplementary figure S3. Observations versus model predictions of bacteria count

Top, middle and bottom panel are bacteria counts for V1SA020 / SH1000, V1SA022 / SH1000, and V1SA019 / USA300 pairs, respectively.

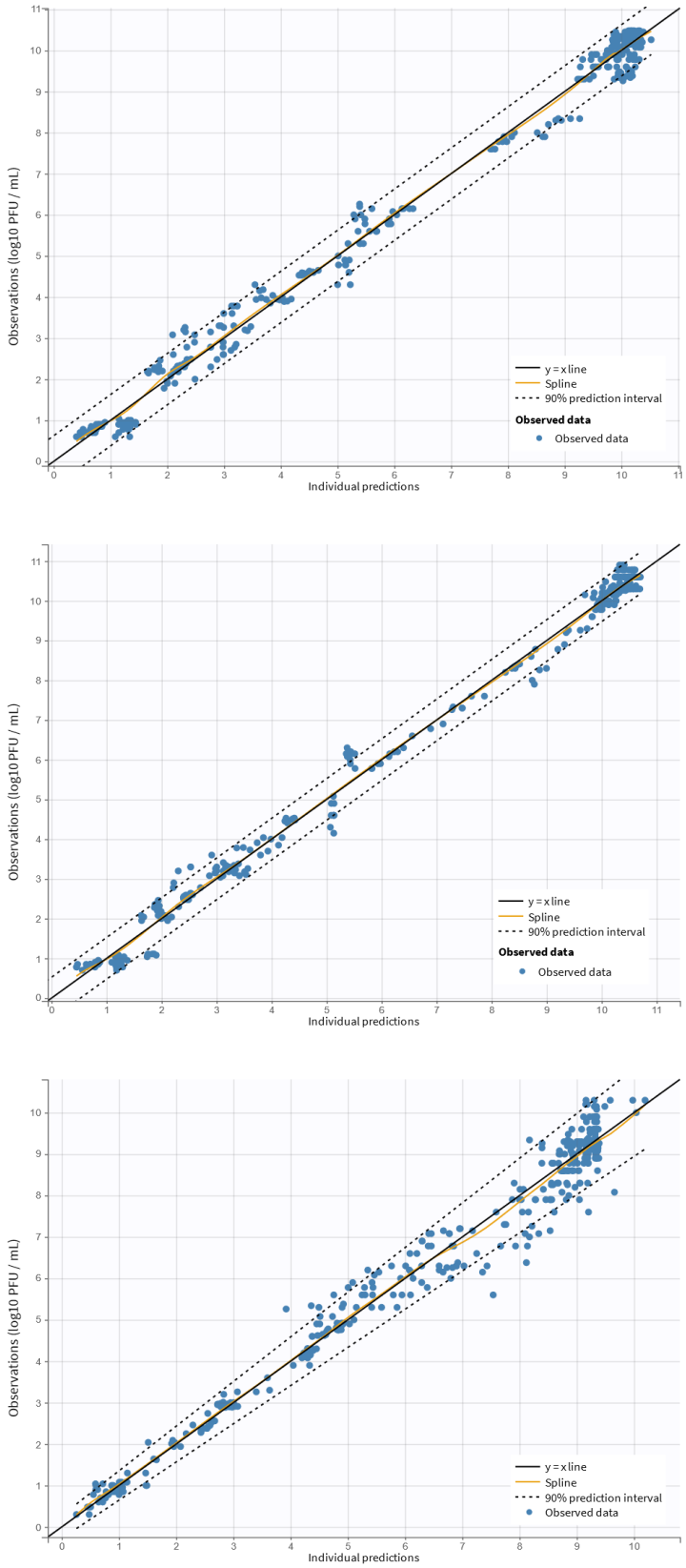

Supplementary figure S4. Observations versus model predictions of phage count

Top, middle and bottom panel are phage counts for V1SA020 / SH1000, V1SA022 / SH1000, and V1SA019 / USA300 pairs, respectively.

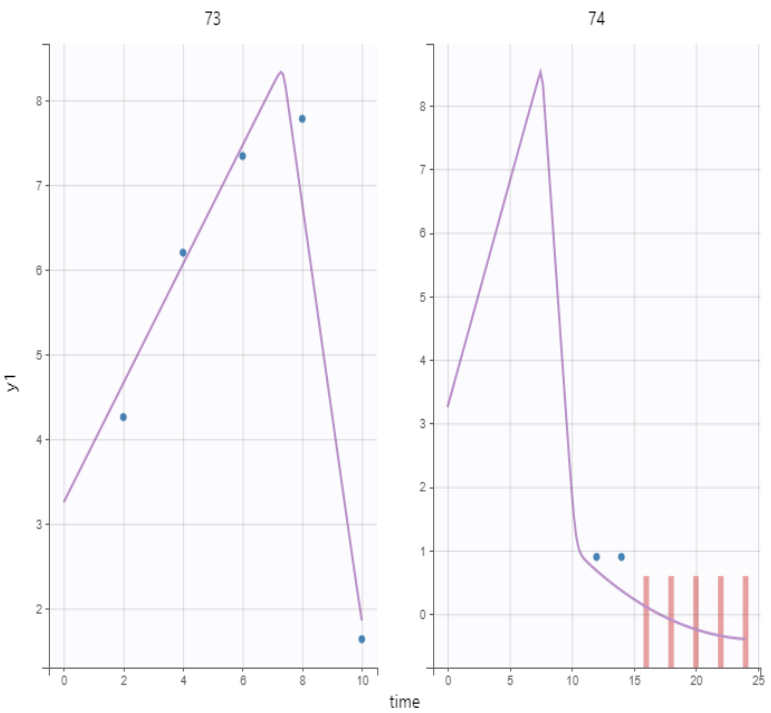
73
74
y1
time

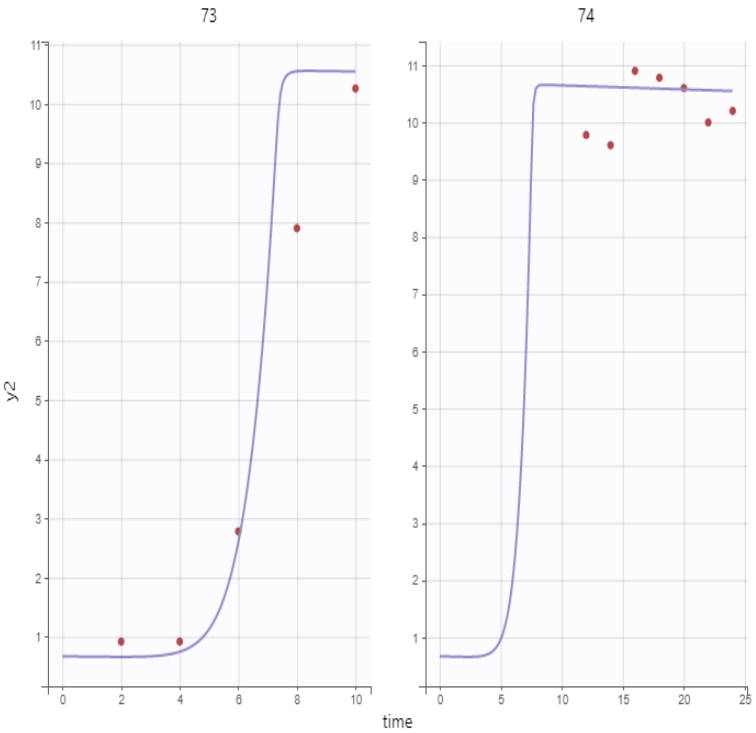
73
74
y2
time

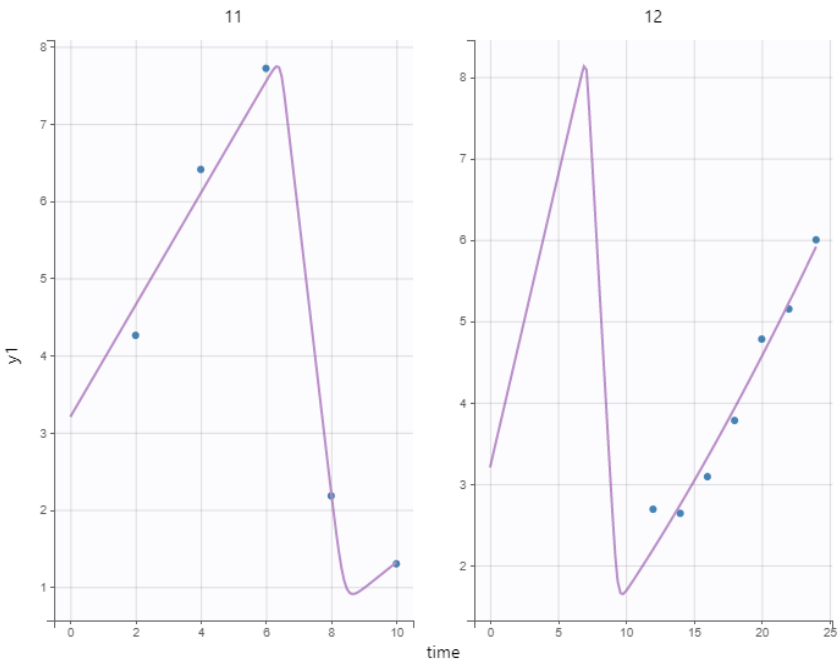
11
12
y1
time

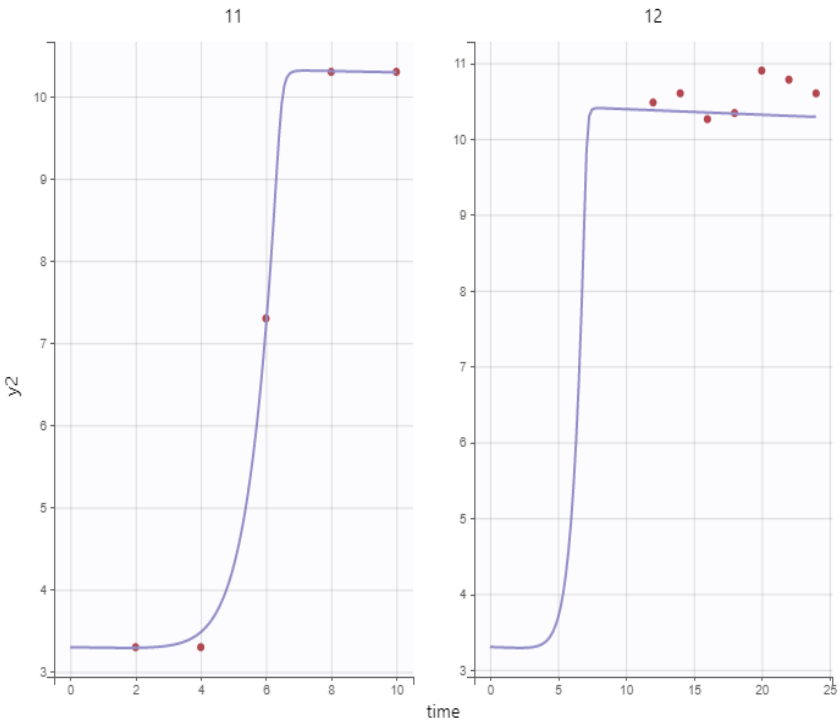
11
12
y2
time

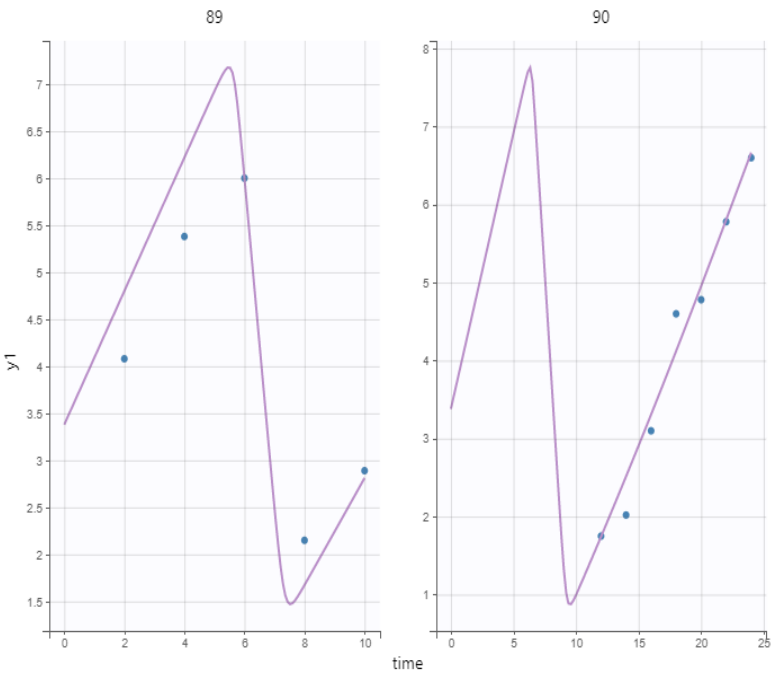

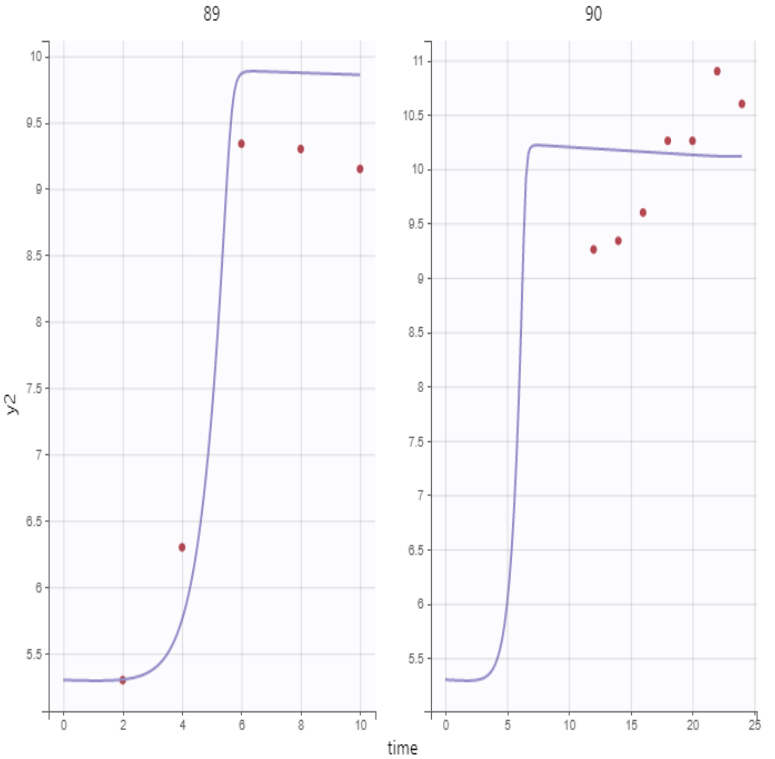

Supplementary Figure S5. Examples of individual fits of bacteria and phage counts for the V1SA019 / SH1000 model

Blue and red dots are bacteria (y1) and phage (y2) counts, respectively. Pink and purple lines are individual model predictions for bacteria and phage, respectively. Red bars indicate observations below the quantification limit.

#73 and 74: B(0) = 1.8E03; V(0) = 5.0E00; MOI initial ≈ 0.01

#11 and 12: B(0) = 1.6E03; V(0) = 2.0E03; MOI initial ≈ 1

#89 and 90: B(0) = 2.4E03; V(0) = 2.0E05; MOI initial ≈ 100

Each pair represents two successive experiments with the same initial conditions and different time windows, 1-10 h and 12-24 h.

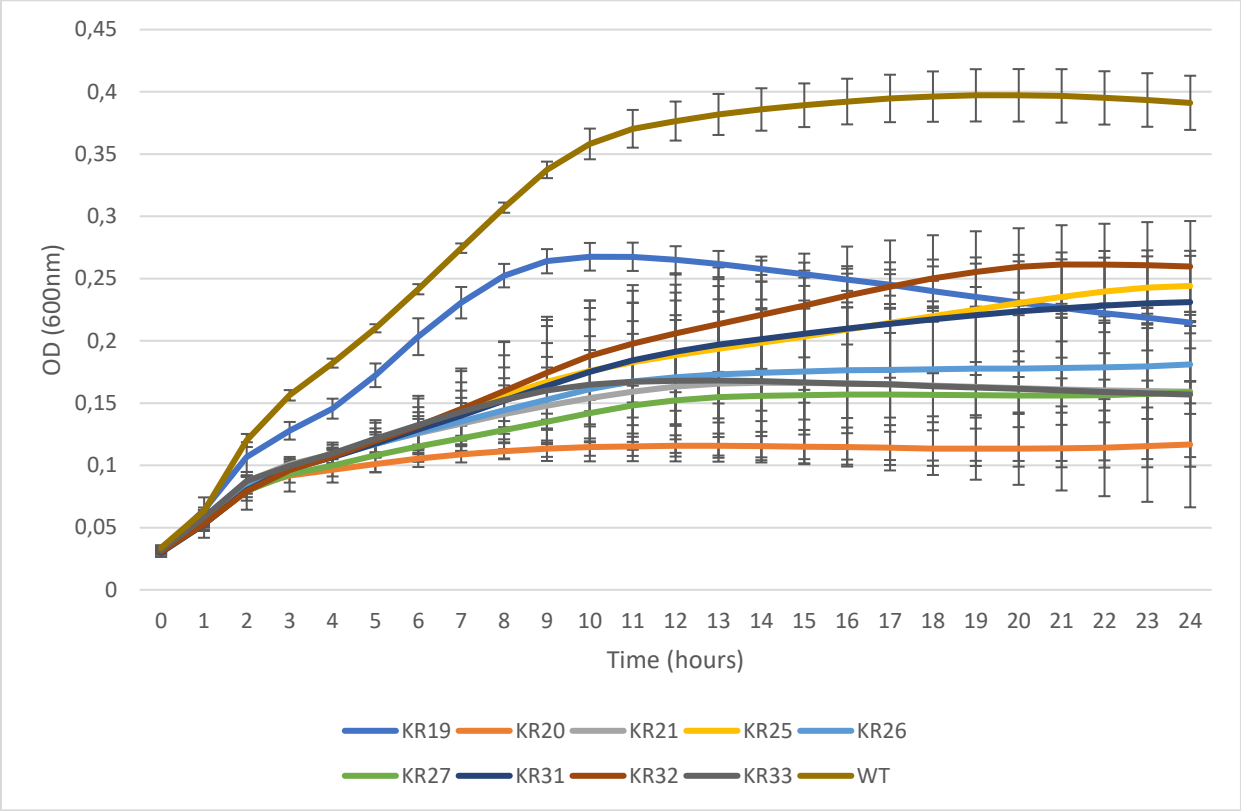

Supplementary Figure S6. Growth curves for SH1000 resistant clones to V1SA019. Bars represent the standard deviation of 4 biological replicates. WT: Wild-type SH1000 strain.